UNIVERSITY OF OKLAHOMA GRADUATE COLLEGE

THE RESPONSE OF MINERAL-ASSOCIATED ORGANIC MATTER TO DROUGHT CONDITIONS AND THE SIGNATURES OF LAND USE IN SEDIMENT LOADING IN CENTRAL OKLAHOMA

A THESIS

SUBMITTED TO THE GRADUATE FACULTY

in partial fulfillment of the requirements for the

Degree of

MASTER OF SCIENCE

By

Brittany Moehnke

Norman, Oklahoma

2025

THE RESPONSE OF MINERAL ASSOCIATED ORGANIC MATTER TO DROUGHT CONDITIONS AND THE SIGNATURES OF LAND USE IN SEDIMENT LOADING IN CENTRAL OKLAHOMA

A THESIS APPROVED FOR

THE SCHOOL OF GEOSCIENCES

BY THE COMMITTEE CONSISTING OF

Dr. Caitlin Hodges, Chair

Dr. Jason Vogel

Dr. Timothy Filley

ACKNOWLEDGEMENTS

I would like to first and foremost thank my advisor Dr. Caitlin Hodges for her unwavering support, her management of a welcoming lab group, and for her enthusiasm regarding critical zone biogeochemistry. Furthermore, I must express my gratitude toward my parents who have always encouraged me to pursue my interests and made my academic pursuits possible. I would also like to thank the members of my committee, Dr. Jason Vogel and Dr. Timothy Filley, for their feedback, knowledge, and support. I thank the United States Department of Agriculture for providing funding the project evaluating the impacts of drought on soil carbon. I deeply appreciate the assistance and support from members of the Hodges Lab, Tiffany Legg, Jacob Clements, Dodger Stankewitz, and Paige Langford, who assisted with field sampling, lab work, other aspects of these projects. Finally, thank you to my fellow graduate students Karen Valles, Mackenzie Flynn, and Danielle Brunig for their friendship and reliability.

TABLE OF CONTENTS

LIST OF TABLES

LIST OF FIGURES

ABSTRACT: Chapter One

Soil organic carbon (SOC) acts as a significant terrestrial carbon sink, and its turnover is a factor of the different pools of SOC in a soil. Mineral-associated organic matter (MAOM) is considered to be a particularly stable SOC pool. MAOM is protected from microbial respiration primarily through strong chemical bonds between the OC and mineral, promoting soil carbon storage. Despite this inherent stability, MAOM turnover has been found to depend upon climatic conditions and the physiochemical properties of a given soil. Thus, there is a need to evaluate MAOM stability across different climates while simultaneously considering the mineralogical controls on MAOM storage. In Central Oklahoma, changes in the amount and frequency of rainfall are anticipated due to climate change. To assess the impact of a changing climate on SOC, we characterized total SOC and MAOM-C in soil samples from a field-manipulated rainfall gradient in an existing temperate prairie. We hypothesized that there would be alterations to total SOC and MAOM-C concentrations in response to a simulated drought experiment. Soils were analyzed following the 4-year DroughtNet experiment at the Kessler Atmospheric and Ecological Field Station in Central Oklahoma. Here, shelters were constructed so that soil plots received a controlled amount of precipitation ranging from 50% addition to 100% exclusion of the natural precipitation. Changes in C concentrations were evaluated following a series of extractions that separate MAOM-C based off the crystallinity of the iron or aluminum oxide to which it was bound. We further hypothesized that the response to precipitation treatments would be evident within these pools of increasingly stable metal species with more crystalline species increasingly holding C in drought conditions. However, no statistically significant relationships were identified between total SOC or MAOM-C pools and precipitation. Still, the most abundant

pools of Fe and Al species were identified as well as to what species most of the MAOM-C was likely bound. We found that soil Fe was mostly in the form of crystalline iron oxides. However, the extractable MAOM-C was preferentially bound to less crystalline Fe species such as short-range order (SRO) Fe-(hydr)oxides or Fe found in the form of organo-metallic associations. Al species were more abundant than Fe species in these less crystalline states. Interestingly, much of the MAOM-C remained following the removal of these reducible metal-oxide species. Using X-ray diffraction, we confirmed the presence mixed layered 2:1 phyllosilicate clays that likely hold the remainder of the C in the < 53 μm MAOM fraction. The preferential adsorption of C to less crystalline, more reactive metal species and clay could result in MAOM vulnerability over a greater timescale. However, the whole soil SOC as well as the MAOM-C fractions appear to be stable across the precipitation gradient and are governed by soil texture rather than moisture.

CHAPTER 1 : CLAY MINERAL SPECIES AND CRYSTALLINITY IMPACT MINERAL-ASSOCIATED ORGANIC MATTER STABILITY ACROSS A PRECIPITATION GRADIENT

1.00 Background

1.00.1 Soil Organic Carbon

Soil Organic Carbon (SOC) is derived from a variety of sources and stored in multiple forms which impact its recalcitrance and thus residence time within a soil. The differences in the resilience and abundance of SOC pools in countless soils have been evaluated, though the parameters defining these C pools have varied (Christensen et al., 2001; Haddix et al., 2020; Helbling et al., 2021; Poeplau et al., 2018). Historically, SOC was divided into pools of humic and fulvic acids for the division between lower and higher molecular weight compounds. However, these two classes were separated through a series of alkaline extractions which chemically altered the OM, essentially rendering this distinction between pools meaningless (Cotrufo & Lavallee, 2021; Lehmann & Kleber, 2015). Therefore, modern convention of separating SOC into dissolved organic matter (DOM), particulate organic matter (POM), and mineral-associated organic matter (MAOM) better accounts for the variety of states in which SOC may actively exist within a soil. These pools are more representative of the continuum of SOM degradation, transport, protection, and biological processing.

The origin of SOC and its state of decomposition impacts the way it integrates into the soil matrix. SOM may be incorporated through plant litter, root exudates, microbial processes,

necromass, and other means. For example, POM is dominated by plant litter residues protected via aggregation rather than by root exudates or other forms of biomass (Cotrufo et al., 2019; Cotrufo & Lavallee, 2021; Just et al., 2023; Rocci et al., 2021). Alternatively, the water-soluble DOM may be transported via pore spaces to serve as microbial substrates or to chemically adsorb or coprecipitate forming MAOM (Chow et al., 2022; Cotrufo & Lavallee, 2021). The laboratory methods and specifications for separating soil fractions into MAOM have varied across studies with some studies separating these pools by density and others by particle size. However, it is widely agreed upon that the MAOM may be operationally defined as < 53 μm in size (Cotrufo et al., 2019; Cotrufo & Lavallee, 2021; Sun et al., 2023). Using this definition, MAOM has been found to have a lower C:N ratio than POM and to be comprised of SOM acting as a substrate often bound within micropores or microaggregates of a variety of mineral species (Cotrufo & Lavallee, 2021; Mirabito & Chambers, 2023). These species range from from poorly crystalline short-range order (SRO) metal (oxy)hydroxides to phyllosilicate clays (Mirabito & Chambers, 2023). MAOM is considered the more stable fraction of organic matter within a soil with its larger turnover time, as opposed to that of POM, due to its combination of physical protection provided through the formation of aggregates and chemical protection via bonding to mineral surfaces. (Cortufo et al., 2019). Due to the slower cycling of MAOM, any perturbations that may cause significant C loss from this pool would yield considerable consequences for the global C cycle. As a result, the evaluation of MAOM stability in the face of climate change is necessary to better our understanding of this potential source of atmospheric carbon.

1.00.2 Mineral-Associated Organic Matter

The study of individual controls on MAOM stability helps to inform how MAOM may respond to changes in climate. For example, previous studies have sought to characterize the effects of fresh DOM inputs carried by precipitation on MAOM destabilization versus formation due to the competing nature of the addition of fresh DOM (Cotrufo et al., 2019; Ritson et al., 2014). This input has been found both to boost microbial activity which can lead to greater CO_2output while also increasing total MAOM by either the fresh inputs directly adsorbing to minerals or by resulting in byproducts of microbial processing binding to mineral surfaces (Cotrufo et al., 2019; Li et al., 2023). The formation and stability of MAOM has also been found to be largely dependent upon the non-litter inputs of SOM and the factors which contribute to the abundance of these sources. These factors are physical, chemical, and biological in nature and are involved in various feedback mechanisms, acting as either controls or catalysts to one another. Biotic components such as symbiotic relationships between plants and mycorrhizal fungi, for example, create a microenvironment which influences the capacity for MAOM formation through the exudation of low molecular weight organic acids which help mine for nutrients such as nitrogen and phosphorus (Andrino et al., 2021; Cotrufo & Lavallee, 2021;Gross & Harrison, 2019). The release of these organic acids has been found to free phosphorous-containing MAOM bound to goethite through mechanisms such as ligand exchange and dissolution (Andrino et al., 2021). This exudation and subsequent reaction are controlled by several factors such as rooting depth, total biomass, and the plant community. While biomass and root exudates are important to MAOM formation and destabilization, the accessibility of MAOM to microbes ultimately determines its turnover rate. As a result, the texture and mineralogy of a

soil exert a great amount of control over microbial access to MAOM and thus to MAOM stability.

1.00.3 Soil Texture as a control on MAOM

The texture of a soil greatly influences its capacity to hold and transport SOM. It has been well established that metal oxides and some clay minerals greatly enhance the potential OM sorption in a soil (Bramble et al., 2024; Coward et al., 2017, 2018; Haddix et al., 2020). This is due to the greater reactive surface area of these minerals (Li et al., 2023; Saidy et al., 2013; Wagai & Mayer, 2007). An abundance of 2:1 phyllosilicate clays, specifically, has been found to promote MAOM retention (Six et al., 2000; Rakhsh et al., 2017). This increase in MAOM stability is due to the high cation exchange capacity (CEC) of 2:1 clays as well as the greater surface area that comes with having a hydrated interlayer in addition to available edge sites (Rakhsh et al., 2017; Saidy et al., 2013; Singh et al., 2017). However, these clays have variable surface charges which are pH dependent. Saidy (2013) confirmed through a series of incubation studies that samples containing 1:1 clay such as kaolinites experienced more C mineralization than those containing smectite and illite which both have greater CEC and SSA than illite.

While hydrated 2:1 clays are more inclined to bind SOC compared to a 1:1 clay, these are also sensitive to changes in soil moisture. A change in precipitation leads to the shrinking or swelling of these clays which in turn alter the interconnectivity of macropores within the soil or lack thereof (Diel et al., 2019; Rasmussen et al., 2006, 2018; Singh et al., 2017; Zafar & Lu, 2015). Interconnected pores allow for the easy diffusion of gas and transport of DOM down a soil profile. In soils with a high concentration of 2:1 clays, significant changes in soil hydrology

can occur due to the formation of cracks upon shrinking and the trapping of moisture upon swelling. This alteration to the soil structure also impacts aggregate stability and the containment of oxygen, water, and microbial communities within aggregate micropores (Menon et al., 2020; Souza et al., 2023). The presence of clay also influences the formation of micro and macroaggregates by acting as a cement between particles, providing additional protection to already chemically bound SOM (Rakhsh et al., 2017; Rasmussen et al., 2018). Soil texture also exerts control over MAOM formation through permeability. On one hand, greater sand content drives leeching which transports DOM further down a profile to accumulate in a horizon with a greater capacity to bind the MAOM. However, within the sandy portion of the soil, protection via occlusion is limited, potentially leaving SOM more vulnerable to microbial attack and subsequent mineralization. As a result, any SOM protection relies heavily on interactions with amorphous iron oxide coatings on the sand grains. These coatings are held by Van der Waals forces and more strongly by Fe-O-Si bonding (Scheidegger et al., 1993, as cited in Giannetta et al., 2018). Further study by Giannetta et al. (2018) confirmed that the coating of sand grains with Fe (III) species increases the reactive SSA but also found that the extent to which the addition of Fe (III) to both the sand and the silt + clay fractions impacted OC stabilization was dependent upon initial SOC content. Here soils with more OC resulted in greater C stabilization through bonding with Fe (oxy)hydroxides (Giannetta et al., 2018). Indeed, the mere presence of an Fe (III) coating does not guarantee enhanced SOM sorption. While initial OC has been found to play a role in determining the amount of MAOM formation, Saidy et al. 2013 found that the addition of a goethite coating to select phyllosilicate clays only significantly enhanced C sorption and SSA in kaolinite which had the lowest initial CEC and SSA. The clays which already were

likely to bind OM were not significantly impacted despite the fact that iron oxides such as goethite are capable of bonding OM through a variety of mechanisms (Saidy et al. 2013).

1.00.4 MAOM stabilization: Metal (oxy)hydroxides

It has been found that the presence of metal oxides (including oxyhydroxides and hydroxides) greatly impacts MAOM presence and stability in soils with a neutral pH (Lopez & Rovira, 2013; Singh et al., 2017). However, the extent of their role in soils with lower initial OC as well as the difference in sensitivity to changing climatic conditions between metal oxide species are both in need of further study (Coward et al., 2018; Heckamn et al., 2017; Patzner et al., 2020). Before analyzing the differences between metal oxides' responses to environmental alteration, the mechanisms underlying their interactions with SOM to form MAOM must be discussed.

MAOM stability is dependent upon the mineral species to which the OM is attached, the functional groups present in the OM, and consequently, the strength of the resulting bonds. The forces contributing to the formation of MAOM include cation bridging to form organometallic complexes, hydrogen bonding, covalent bonds directly with metal oxides, ligand exchange, co-precipitation, and Van der Waals forces. The complexity or crystallinity of the mineral species dictates the means of association (Boudot et al., 1989; Li et al., 2023; Singh et al., 2017). OM that is directly bound to the mineral surface is the most protected, while more distal organic matter is more subject to desorption depending on environmental factors (Kleber et al., 2007). Additionally, a higher C input into the soil impacts protection by comprising of these outer reactive zones that are more accessible to microbes.

281

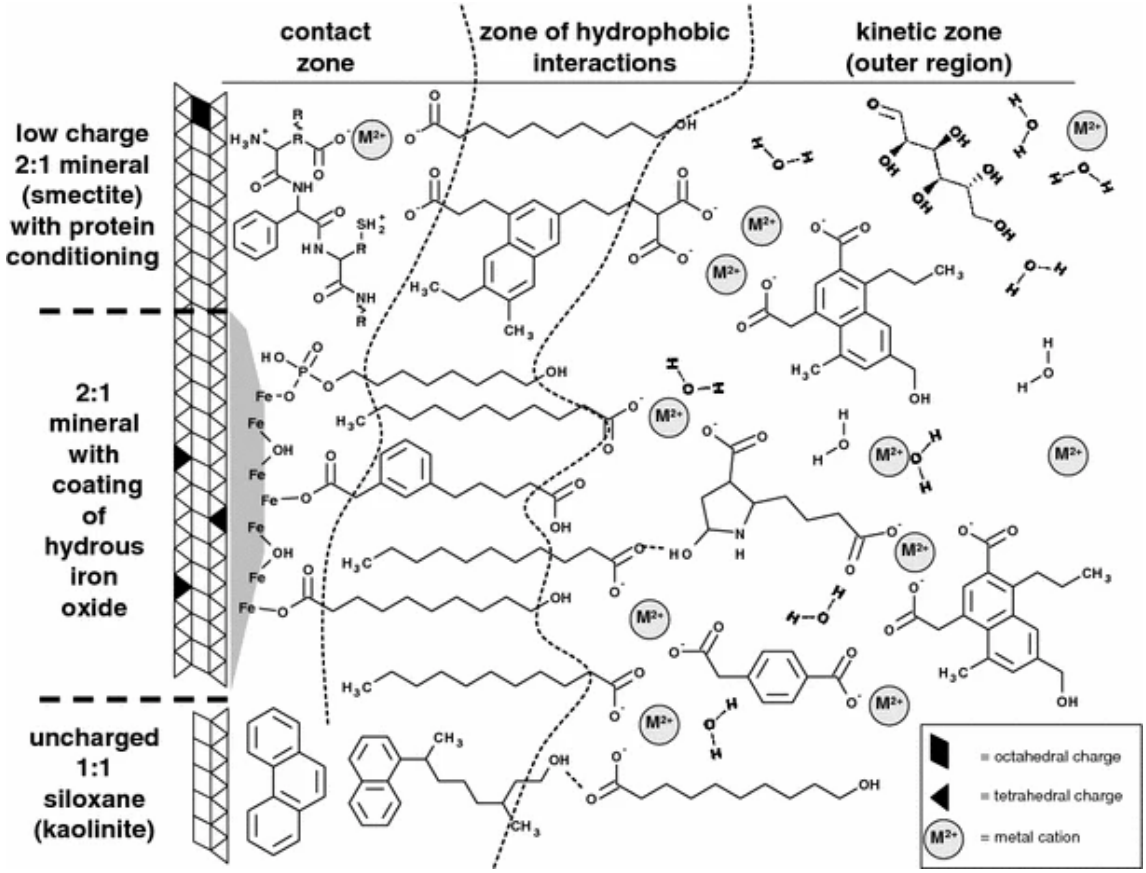

Figure 1) Zonal model of MAOM (Kleber et al., 2007)

282

283

284 1.00.5 Targeted Extractions of Iron (oxy)hydroxides

285 Due to the variety of iron oxides found in soil in terms of their crystallinity, surface area,
286 and reactivity, methods targeting different pools of these species have been developed. These
287 targeted extractions have been used to determine if organic carbon is found in association with

reactive, more easily reduced Fe or Al-containing minerals or bound to more stable crystalline species found in soil.

The extraction solution that is typically used first is sodium pyrophosphate (Fox et al., 2017; Heckman et al., 2018). This solution targets free Fe or Fe in loose associations with organic matter. However, it is not a strong enough oxidant to reduce iron-bearing minerals. Hydroxylamine-HCl has been utilized to extract more easily reduced, short-range order (SRO) iron and aluminum oxides (Fox et al., 2017; Gabriel et al. 2018; Heckman et al., 2018). Lastly, the third extraction using a sodium dithionite solution, developed by Wagai & Mayer, 2007, has been applied as an inorganic alternative to using citrate bicarbonate to target the most crystalline iron oxides and oxyhydroxides present in soil, such as hematite and goethite (Gabriel et al. 2018; Heckman et al., 2018).

How precisely these extractions isolate the specific pools attributed to each has been subject to debate and further study. Multiple studies have postulated that there is some overlap between targeted mineral pools. One challenge in determining the accuracy of the stated function of each target extraction lies in the difficulties faced in imaging SRO minerals. While X-ray diffraction can be effectively implemented to identify even randomly ordered minerals present, its capacity to identify SRO iron oxides is severely limited, especially when bound to OM. This is largely attributed to their amorphous nature as well as the destructive techniques required to remove OM interference (Allegretta et al, 2022; Dohnalkova et al., 2022). A variety of techniques have been applied to study interactions of OM at the mineral surface including Fourier transform infrared spectromicroscopy (SR-FTIR) as well as near-edge X-ray absorption fine structure (NEXAFS), but these techniques are more effective for identifying speciation of organic compounds and interactions at micro to nano interfaces as opposed to wider distribution

across a spatial scale or between different iron (oxy)hydroxide species (Li et al., 2023). Additionally, it has been found that overlap between absorption bands particularly in regard to O-H and Si-O-Si stretching can make even differentiation between inorganic and organic species a challenge when using SR-FTIR (Li et al., 2023). This limitation leads to the necessity of looking at OM, SRO Fe (oxy)hydroxides, and soil mineralogy using a combination of several methods.

A study conducted by Slotznick et al, 2019 utilized X-ray diffraction in conjunction with methods evaluating sample magnetism, along with the detection of dissolved iron using the ferrozine method developed by Stookey (1970) to determine the accuracy of targeted extractions in terms of identifying dissolved iron-bearing minerals from sediments using sodium acetate, 1 M hydroxylamine-HCl in acetic acid, sodium dithionite solution buffered with acetic acid and sodium citrate, and ammonium oxalate. Notably, these extractions were C-containing, as evaluation of MAOM was not a concern. Regardless, it was found that sodium dithionite efficiently extracted the expected targeted minerals of hematite and especially geothite. On the other hand, while hydroxylamine-HCl did not target more crystalline species, some overlap occurred in dissolution of more easily reduced Fe species between the previous sodium acetate extraction and the hydroxylamine-HCl (Slotznick et al, 2019). Additionally, the effectiveness of these targeted extractions has been found to depend upon physiochemical properties of the soil itself. For example, the parent material impacts the reactive surface area available which in turn impacts the effectiveness of an extraction (Poeplau et al., 2018). Furthermore, while some studies have successfully characterized C content in each extraction pool across different soil types, differences in these C concentrations could be associated with properties such as the pH of the soil or its buffering capacity as these chemical properties are drivers of metal oxide dissolution

(Heckman et al., 2018; Boudot et al., 1989). The measurement of large changes in C concentration following each extraction has also been associated with initial soil OM content and total soil N (Heckman et al., 2018; Waigai et al., 2011). In conclusion, the targetability of Fe and Al species based on crystallinity and reducibility has been found to be reliable but not necessarily exact with regards to SRO species.

1.00.6 Statement of Purpose

Here, we hypothesize that a 4-year drought simulation results in total SOC and MAOM concentrations that correlate to the amount of precipitation received. Moreover, we expect that by using sequential carbon-free extractions that target reducible metal species, we can identify the Fe and Al species to which C may be bound within the MAOM fraction of a soil. We hypothesize that the change in C concentration between these MAOM fractions also responds to these precipitation treatments.

1.01 Methods

1.01.1 Field Site and DroughtNet Experimental Design

Archived soil samples from depths 0-15 cm and 30-45 cm were acquired from the DroughtNet experiment held at the Kessler Atmospheric and Ecological Field Station (KAEFS, http://kaefs.ou.edu/), central Oklahoma, USA (34°59'N, 97°31'W). Previous studies at this site assessed the change in plant communities in drought conditions where acrylic panels were utilized to divert precipitation from specified plots as well as feed additional rainfall into others.

This created an array of sites with varying total precipitation inputs from 100% exclusion of precipitation to −80%, −60%, −40%, −20% , natural precipitation conditions, and 50% addition. There were 3 plots for each precipitation treatment, resulting in a maximum of 3 samples per precipitation treatment at each depth. The DroughtNet study started in 2016 with the soils sampled at the conclusion of this experiment in 2020. The total average annual rainfall over the course of this experiment was 1132 mm with a range from 992.1 mm in 2017 to 1,241 mm in 2018. The soil samples were previously stated to be classified as a Nash-Lucien complex which are Udic Haplustolls with a near neutral pH and a water holding capacity of 37% (Xu et al., 2013, as cited in Castillioni et al., 2020).

1.01.2 Soil Fractionation

The soils were sampled in 2020, air dried and stored at room temperature. A subsample of each was milled to a fine powder and analyzed for total carbon using the organic elemental analyzer vario El cube. We manually disaggregated the soils and ran the samples through a 2mm sieve. 5 g subsamples of this soil were then acquired to isolate the MAOM fraction (< 53 μm). A size-based fractionation method was selected to isolate this fraction because it is widely used and has been found to be reproduceable and efficient compared to other methods (Haddix et al., 2020; Poeplau et al., 2018; Coward et al., 2017, 2018; Sun et al., 2023). The 5g subsamples were each shaken in in 0.5% sodium hexametaphosphate with glass beads in a lateral orientation for 18h to disperse the soil. Samples were rinsed, placed in drying pans, and oven dried at 60 °C, crushed using a ceramic mortar and pestle, then run through a 53 μm sieve.

1.01.3 Selective Dissolution Extractions

The < 53 µm fraction of the soil, here named the MAOM fraction, was next separated into three subfractions through a series of selective dissolution extractions aimed at separating iron and aluminum species by their crystallinity and thus freeing the organic carbon bound to the species targeted by each extraction. The sequential extraction method, as used by Heckman et al. (2018), is a series of carbon-free extracts that target different pools of metal-bound SOM including the sodium dithionite-HCl extraction originally developed by Wagai & Mayer (2007) to replace the commonly used carbon-containing citrate bicarbonate extractant. The first extractant used was sodium pyrophosphate, which targets loosely bound metals found in organometallic associations and complexes. The second, hydroxylamine, targets poorly crystalline iron and aluminum oxides. The third extractant, sodium dithionite, targets crystalline targets crystalline species Fe and Al oxides. Therefore, this sequential technique allows for better identification of the mechanism of MAOM stabilization. The C concentration of the soil following the pyrophosphate extraction identifies the clay + metal oxide-associated MAOM-C concentration, the post-hydroxylamine C concentrations include the MAOM-C held by crystalline metal oxides and clay, and the post-dithionite concentration of C represents the clay-associated concentration of MAOM-C.

We weighed 1 g of each MAOM sample in pre-weighed centrifuge tubes with 40 mL of 0.1 M Na-pyrophosphate. This first extraction served the purpose of extracting non-crystalline organometallic complexes, namely organic compounds bound to aluminum and iron. The samples were vortexed, then shaken over 18 h. Following the allotted time, we centrifuged the samples for 2h at 5300 RCF. The supernatant was then removed using a syringe with a 0.2 micron filter and transferred into a new 50 mL tube. 5 mL of ultrapure water was pulled through

the filtered syringe and emptied into the tube containing the soil to limit mass loss. The soil was then dried at 60 °C, weighed, and hand homogenized. A 0.2 g subsample was taken before following with the next extraction. This same process was repeated with 40 mL of 0.1 M hydroxylamine in 0.25 N HCl as well as with 30 mL of 0.5 M Na-dithionite. Prior to rinsing with ultrapure water following the Na-dithionite extraction, 10mL of 0.05 N HCl was added to buffer the pH to near 4.8 which prevented any precipitants from forming.

1.01.4 Carbon Measurements

The dried subsamples were packaged in tin boats and analyzed for total carbon. We then used the total carbon concentration in the known sample mass to calculate the mass of C remaining after each extraction with the assumption that the average of duplicate subsample concentrations was representative of the whole. Additional samples from the dried whole < 53 μm fraction of the soil as well as the fraction following the Na-pyrophosphate extraction were acidified using additions of HCl over heat to remove any pedogenic carbonates, a procedure modified from Harris et al., 2021. This serves to compare TC and TOC concentrations between the whole soil and the MAOM-sized fraction. Carbon-free pedogenic carbonate removal treatments using repeated additions of concentrated HCl and heating significantly alter soil pH and Fe oxide speciation and crystallinity which exert strong controls on SOM sorption. As such, carbonate removal treatments were not applied to whole samples prior to the sequential extraction procedure.

1.01.5 X-ray diffraction

X-ray diffraction is a spectroscopic method of characterizing the mineralogy of a sample. For whole sample characterization, a powdered, random sample mount is often applied. When isolating a particular fraction of a fine grain size, such as clay minerals, an oriented mount may be utilized. The oriented mount method was selected and executed according to the procedure listed in Moore and Reynolds, 1997. The clay was separated using sonification in a sodium hexametaphosphate solution. The sonicated sample was centrifuged at 800 rpm for 3.5 minutes to separate the > 2 μm fraction of the sample and leave the clay-sized fraction suspended in solution. The supernatant was decanted and washed with a calcium chloride solution as it was vacuum-filtered to form an oriented-mount on filter paper. The sample was then transferred onto a glass slide, and the filter paper was removed after drying. After the untreated oriented mount was run in the XRD, it was placed in a desiccator containing ethylene glycol overnight and re-analyzed using the XRD. Finally, after the ethylene glycol-treated sample was processed, the oriented mount was placed in the oven at 550 °C for 1 hour, and re-run on the XRD. These treatments to the clay minerals allow for differentiation between clays with overlapping XRD signals by altering the d spacing through the inflation of the interlayer in 2:1 clays or by destruction of the signal for certain clays by heat alteration. Samples were analyzed via X-ray diffraction using a Rigaku Ultima IV powder X-ray diffractometer with a voltage of 40 kV and 44 mA current.

1.01.6 Total Dissolved Metals Measurements

The concentration of dissolved trace metals present in a 1:50 v/v dilution of each solution following extraction were measured via Inductively coupled plasma optical emission

spectroscopy (Thermo Scientific iCap Pro ICP-OES). This concentration was then used to calculate the amount of Fe and Al in the whole volume of each respective extraction solution in order to quantify the amount extracted from each pool.

1.02 Results

1.02.1 Total Carbon versus Precipitation at each Depth

Carbon concentrations for the whole soil fraction were not consistent within treatment groups (Figure 2). The TC content in samples receiving natural precipitation ranged from 14.9 to 23.5 mg C g^{-1} soil for soil at 0-15 cm depth and 16.5 to 17.4 mg C g^{-1} at 30-45 cm (Figure 2). The TOC concentrations ranged greatly as well from 10.4 to 19.3 mg C g^{-1} at 0-15 cm but were greatly reduced to values between 6.3 and 7.2 mg C g^{-1} in the deeper soils (Figure 2). In soils that received no precipitation, the 0-15 cm TC concentrations were from 14.5 to 26.7 mg g^{-1} and TOC was 13.0 to 18.6 mg g^{-1}. The soil from depths of 30-45 cm showed a greater difference in TC and TOC values with TC from 18.3 to 29.1 mg C g^{-1} and TOC from 13.0 to 18.6 mg C g^{-1}(Figure 2). Other treatments including the removal of some percentage of precipitation also showed lower TOC at greater depth and a larger difference between TC and TOC in the 30-45 cm depth soils. Soil with additional precipitation had TC concentrations from 18.0 to 26.6 mg g^{-1} and TOC concentrations of 15.6 to 17.1 mg g^{-1} (0-15 cm) as well notably lower C values in the 30-45 cm soil, 7.1 to 8.6 mg C g^{-1} soil and 2.8 to 3.0 mg OC/ g soil (Figure 2). The large spread in C concentrations within treatments left any relationship between precipitation and C content unclear when evaluating the whole soils consisting of both the POM and MAOM fractions.

The same parameters were next evaluated in the < 53 m sized soil fraction to determine whether changes in precipitation input impacted MAOM content (Figure 3). In the samples receiving natural precipitation, the TC values in the < 53 m fraction ranged from 7.6 to 11. 3 mg C g^{-1} soil at a depth of 0-15 cm and 7.9 to 10.2 mg C g^{-1} at 30-45 cm depths. Following treatment with HCl, these values decreased ranging from 5.9 mg C g^{-1} soil to 9.1 mg C g^{-1} at 0 -15 cm and 4.2 to 5.1 mg C g^{-1} at the greater depth (Figure 3). For the treatment group with the complete removal of precipitation, the TC concentrations ranged from 8.8 to 18.4 mg C g^{-1} soil in the MAOM fraction. The TOC concentrations fell between 6.4 to 10.4 mg g^{-1}. At the 30 – 45 cm depth, TC was from 15.3 to 15.6 mg C g^{-1} C, and TOC greatly decreased with values from 2.0 to 5.9 mg C g^{-1} (Figure 3). In treatments with 50 % addition, the TC was between 6.9 and 17.5 mg C g^{-1} soil at 0-15 cm and 3.4 to 5.2 mg g^{-1} at 30- 45 cm. The TOC values ranged from 5.9 to 7.3 mg C g^{-1} soil (0-15 cm) and 1.9 to 4.0 mg C g^{-1} (30- 45) (Figure 3). The greatest variability was seen within the TC concentrations in treatment groups with complete removal of precipitation. There was a large range of C concentrations for plots within the same treatment groups, showing no relationship between precipitation treatment and total C nor OC in the MAOM fraction.

483

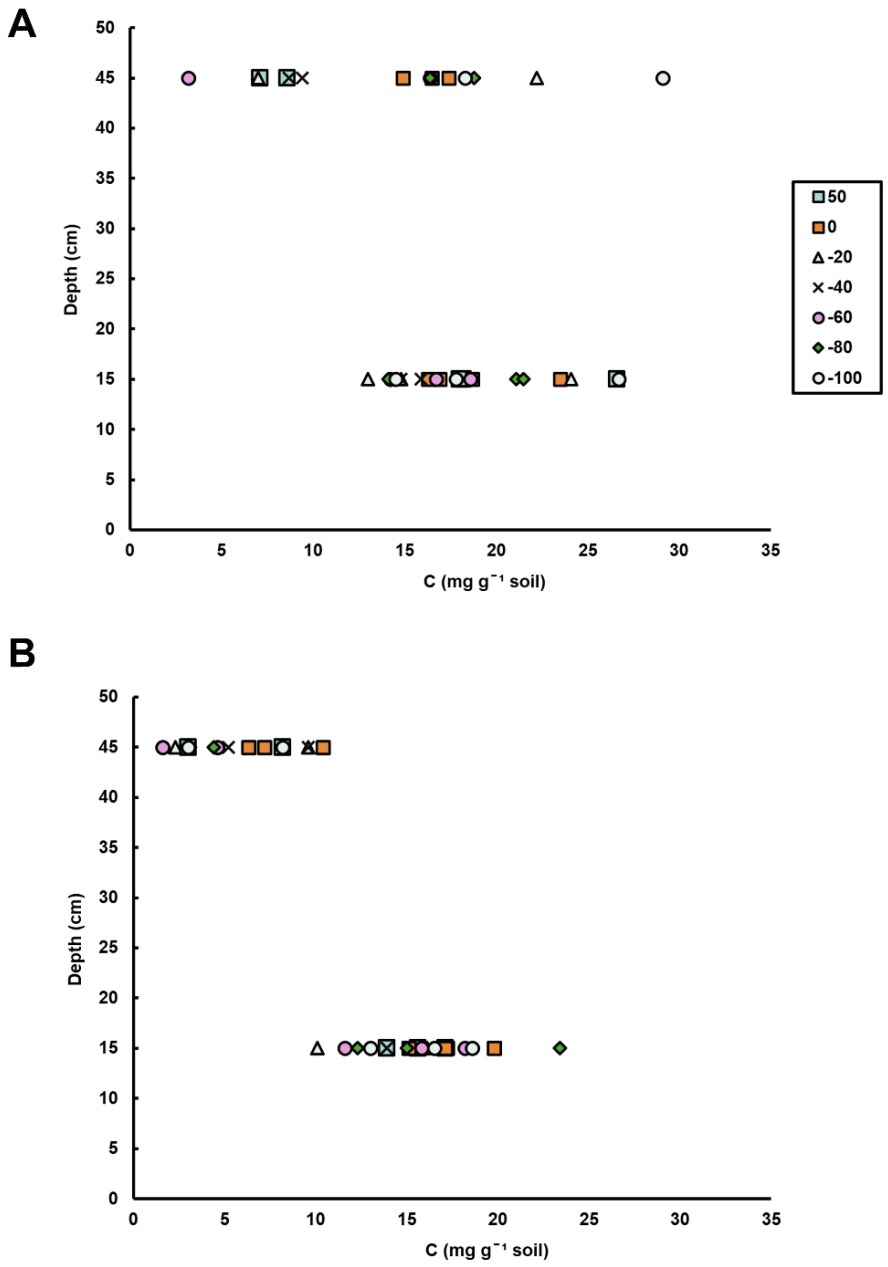

Figure 2) a) Total carbon concentration for whole soil for each precipitation treatment fraction at two depths, 0-15 and 30-45 cm. **b)** Total organic carbon concentration for whole soil samples for each precipitation treatment fraction at 0-15 and 30-45 cm. TOC values are more similar across treatments for both depths than TC.

484

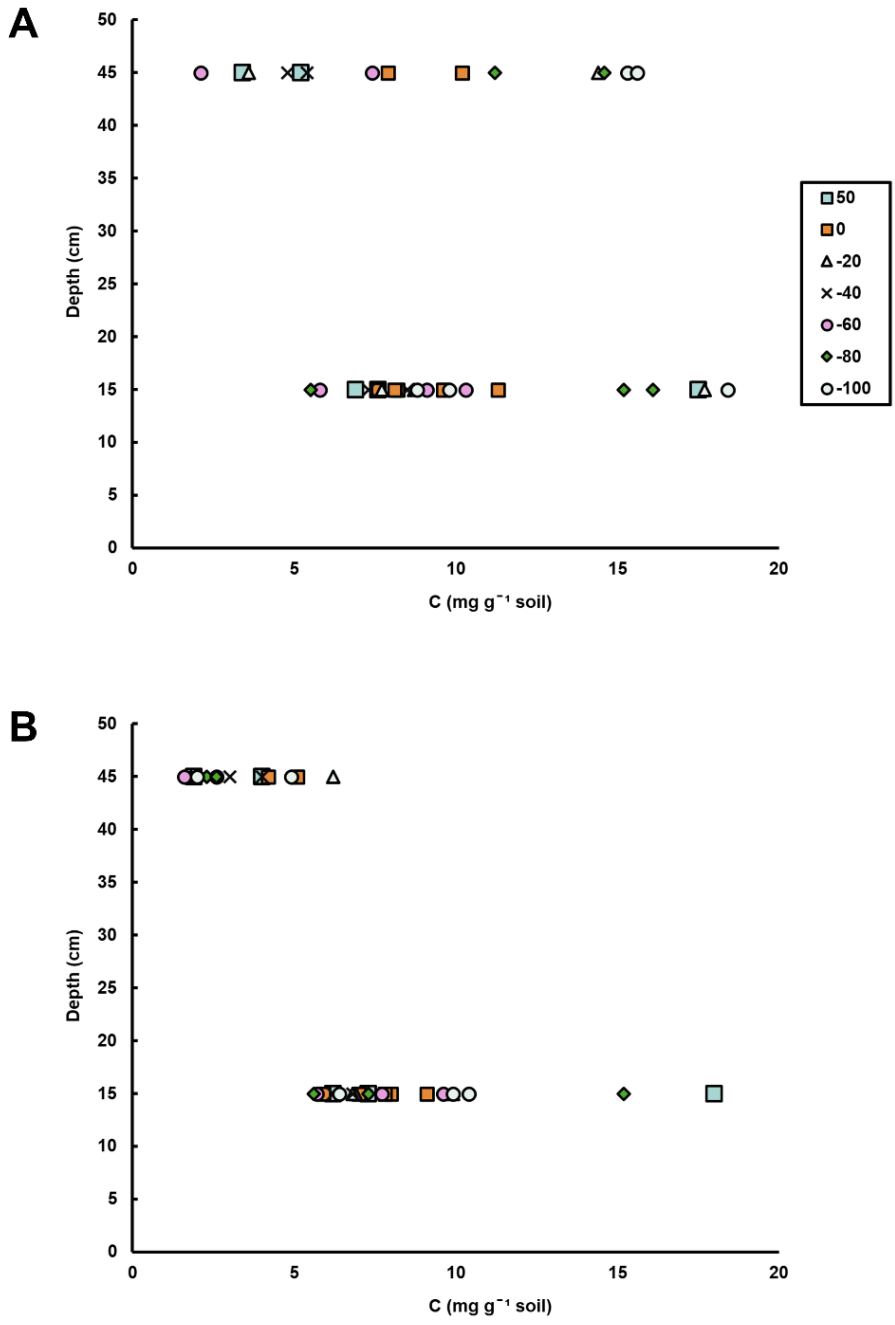

Figure 3) a) Total carbon concentration for <53 µm soil fraction for each precipitation treatment fraction at two depths, 0-15 and 30-45 cm. **b)** Total organic carbon concentration for <53 µm soil fraction for each precipitation treatment fraction at 0-15 and 30-45 cm. In some plots C concentration decreased by over 50% following the removal of IC.

1.02.2 Selective Dissolution Extractions Iron and Aluminum

Next, the change in carbon concentration following each extraction targeting first organometallic associations then different metal oxide phases was evaluated for each plot at both depths (Figures 4, 5). While the initial C concentration in plots receiving the natural precipitation ranged from 7.6 to 11.3 mg g^{-1} in the surface soils (Figure 4) and 7.9 to 10.2 mg g^{-1} in the deeper soils (Figure 5), the concentration of C decreased following the removal of organometallic associations in all but one plot, which increased from 7.57 to 8.60 mg C g^{-1} soil. In the plot with an increase in C concentration following the sodium pyrophosphate extraction, the difference in concentration following the removal of SRO metal oxides was also greater than other plots of the same precipitation treatment (Figures 4, 5). In these plots which received the natural precipitation, concentrations ranged from 4.7 to 6.4 mg C g^{-1} soil at 0-15 cm and 4.8 to 5.1 mg C g^{-1} at 30 – 45 cm. Following the removal of crystalline metal oxides, leaving clays binding OM, the concentration of C ranged from 1.2 to 7.20 mg g^{-1} soil at 0-15 cm and 3.63 to 4.14 mg g^{-1} at 30- 45 cm. In all plots receiving the natural precipitation treatment, the concentration of carbon following the removal of the dithionite extractable C was the lowest (Figures 4, 5).

In samples with 100% absence of precipitation, all but one showed an increase in concentration following the removal of organometallic associations. At 0-15 cm, the concentrations of C following the sodium pyrophosphate extraction ranged from 6.0 to 15.5 mg g^{-1} (Figure 4). C concentrations were 7.4 to 12.2 mg g^{-1} at 30- 45 cm for individual plots with complete removal of precipitation (Figure 5). Following the removal of SRO species with hydroxylamine, the concentrations ranged from 7.0 to 15.5 mg C g^{-1} soil at 0-15 cm and from 6.2 to 9.0 mg g^{-1} at 30 to 45 cm (Figures 4, 5). While the concentrations decreased in

individual plots at 30 – 45 cm following this extraction in the -100% precipitation treatment group, the concentration change was more irregular at 0-15 cm (Figure 4). In one of these plots the change in C concentration was as low as 0.02 $mg\ g^{-1}$. After extracting crystalline species with dithionite, the concentration of C in the -100% precipitation group decreased in all but one plot in the 30-45 cm depth soil which remained nearly unchanged (Figure 5).

In all other precipitation removal treatments (-20% to -80%), the C concentration also decreased following the sodium dithionite extraction, when all organometallic, SRO, and crystalline metal oxide species were removed (Figures 4, 5). However, more variation is seen in C concentration between plots after the removal of organometallic species and SRO metal oxides. Following the pyrophosphate and the hydroxylamine hydrochloride extractions, there is a mixture of soils increasing and decreasing in C concentrations. Furthermore, the plots that received 50% addition of precipitation had changes in C concentration that showed a decrease following the removal of organometallic associations in all plots except one which increased by 0.40 mg C g^{-1} at 0-15 cm (Figure 4). After the removal of SRO species, the concentration of C decreased in all plots with an addition of 50% the natural precipitation then decreased further with the removal of crystalline metal oxide species via sodium dithionite.

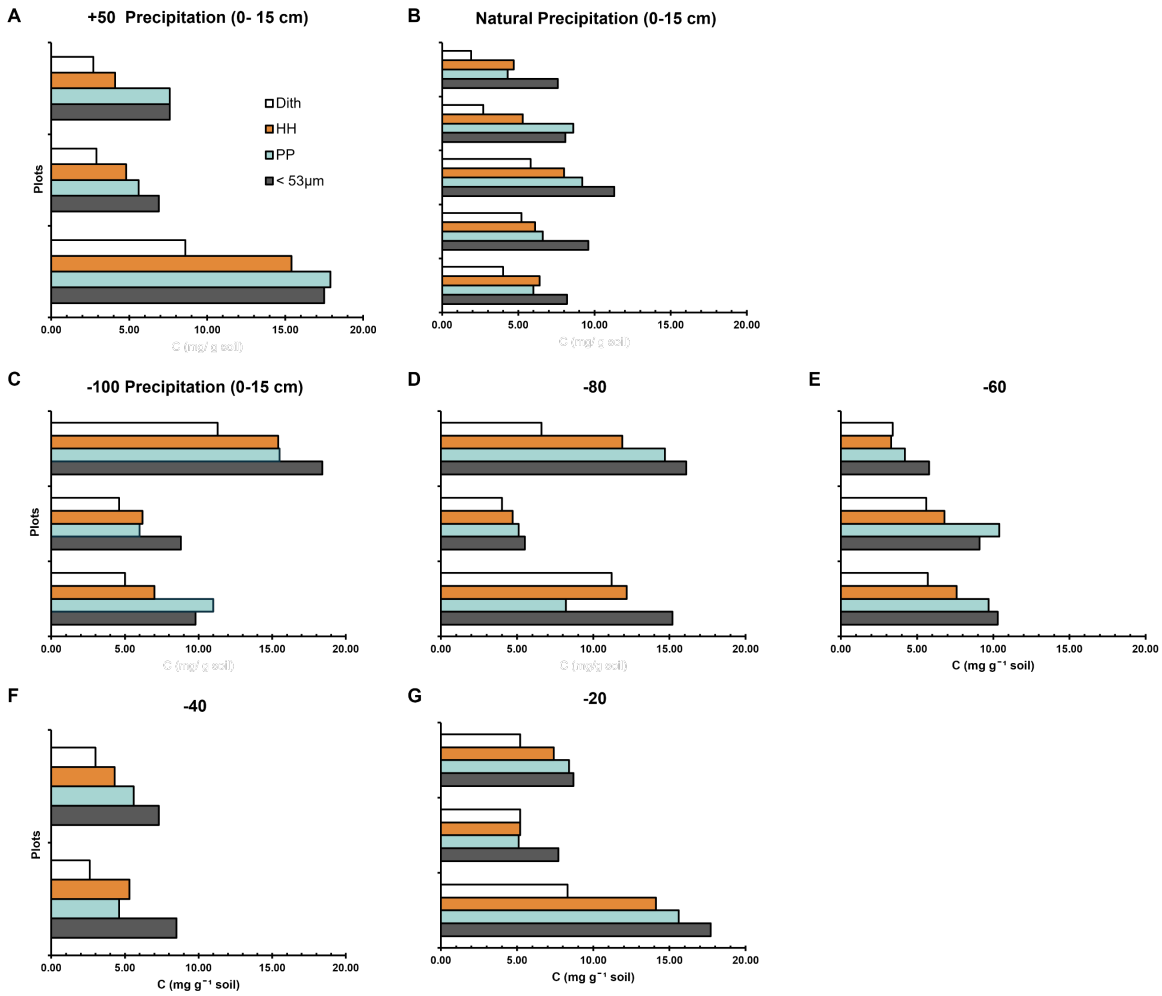

Figure 4) Change in C concentrations for the < 53µm fraction of the upper 0-15 cm soils of individual drought manipulated plots following targeted extractions, grouped by percent of natural precipitation received where **a)** + 50% **b)** natural precipitation **c)** -100 **d)** -80 **e)** -60 **f)** -40 **g)** -20. "PP" represents soils following the extraction using Na-pyrophosphate, "HH" is after hydroxylamine, and "Dith" is following Na-dithionite. The overall C concentration decreased following the removal of both amorphous and crystalline Fe and Al species in all plots, but no relationship with precipitation was identified.

524

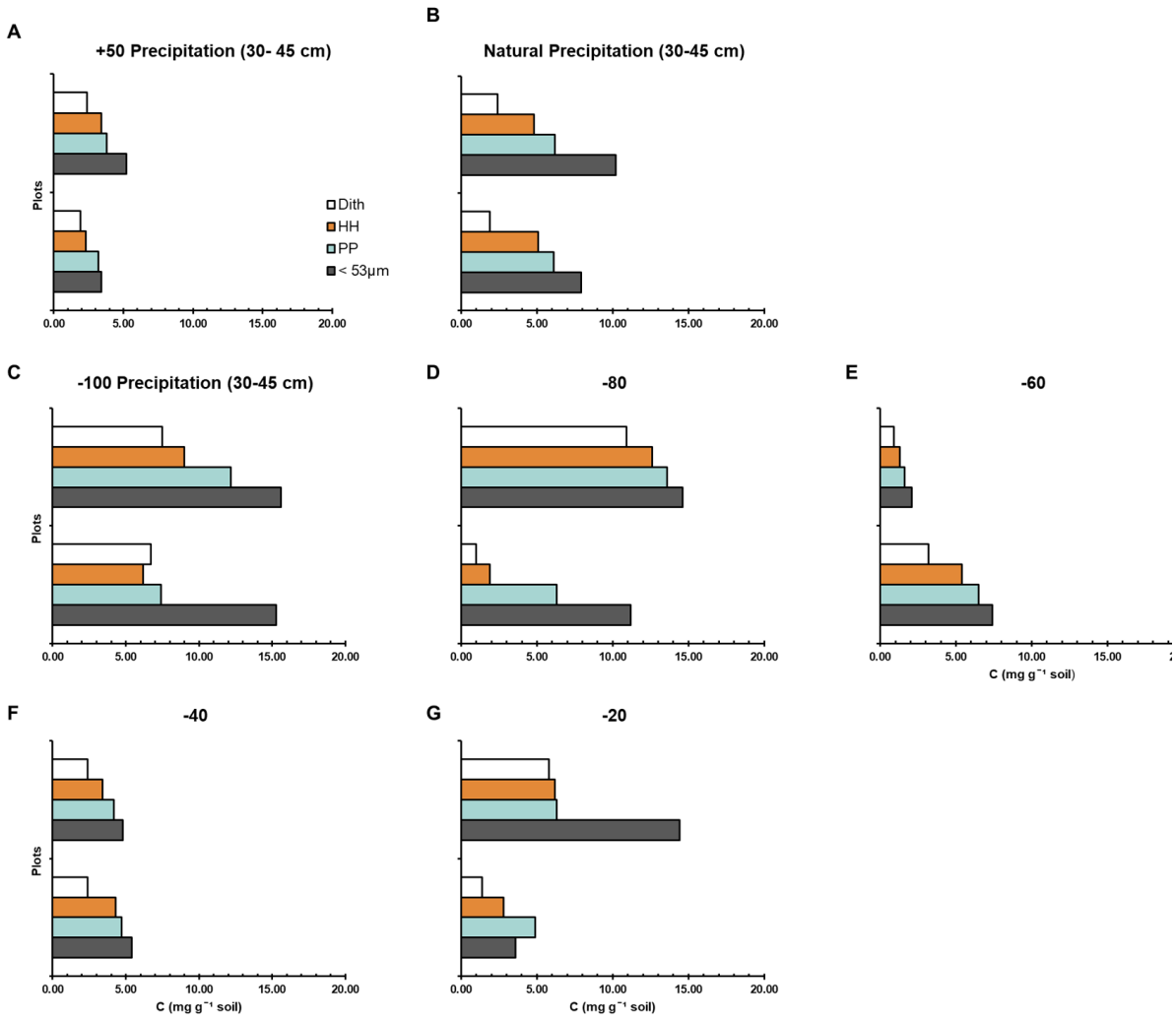

Figure 5) Change in C concentrations for the < 53µm fraction of the 30-45 cm depth soils of individual drought manipulated plots following targeted extractions, **a)** + 50% precipitation **b)** natural precipitation **c)** -100 **d)** -80 **e)** -60 **f)** -40 **g)** -20. The initial C concentrations were generally lower than those of the 0-15 cm depths but showed the same variation between individual plots of the same treatment group. The remaining C concentration following all extractions was less that the initial concentration.

525

526

1.02.3 Dissolved Fe and Al

In all the 0-15 cm soil samples, the total average Fe removed per g of the of <53 μm soil fraction by sodium pyrophosphate and hydroxylamine were much lower than the concentration extracted by sodium dithionite, regardless of the precipitation treatment group (Figure 6). The average Fe concentrations were also higher for Na-pyrophosphate extractable Fe than the hydroxylamine extractable iron within the same treatment group. The average Na-pyrophosphate extractable iron concentrations were lowest within the 80 percent removal group at 0.050 mg Fe per g of soil and highest in the -100 percent precipitation group at 0.12 mg Fe g^{-1} soil (Figure 6). The -100 percent precipitation group also contained the greatest concentration of hydroxylamine-extractable Fe with a concentration of 0.10 mg g^{-1} soil. The average of the dithionite-extractable Fe between all precipitation treatment groups was 4.15 mg g^{-1} ($\sigma = 0.48$) showing much of the total Fe was in the form of a crystalline iron oxide. The +50 percent precipitation treatment had the highest concentration of Fe within any of the of < 53 μm surface soil extractions at 4.97 mg Fe g^{-1} soil (Figures 6, 7). However, no relationship between the iron concentrations in any extraction and precipitation was identifiable (Figures 6, 7). The concentration of Na-pyrophosphate- extractable Al was much higher than that of Fe in all treatment groups with the molar ratio of Al : Fe ranging from approximately 5:1 to 16:1 (Figure 10). Within the hydroxylamine extraction, slightly lower Al : Fe values were seen, between 2:1 and 10:1. Like the Fe extracted in the 0-15 cm soils, a higher average concentration of Al was extracted by Na-pyrophosphate than was by hydroxylamine in all treatment groups (Figure 10). The average concentration of Al extracted across treatment groups was 0.34 mg g^{-1} soil ($\sigma =$ 0.04) in sodium pyrophosphate extractions and 0.12 mg g^{-1} soil ($\sigma = 0.05$) in hydroxylamine extractions (Figures 8, 9). Interestingly, the Al : Fe relationship was inversed in the dithionite

550 extraction relative to the previous two extractions. The molar Fe concentration ranged from 4 to
551 9 times that of Al (Figure 10). A similar pattern is seen within deeper soils as well.

552 In the 30-45 cm samples, the total Fe pulled by the sodium pyrophosphate was on
553 average 0.025 mg Fe per g of <53 μm soil fraction with a standard deviation of 0.01 and showed
554 no relationship with the amount of precipitation received. The amount of Al pulled by this
555 extraction was greater than Fe also with no clear dependency on precipitation with an average of
556 0.33 $mg\ g^{-1}$ soil and a standard deviation of 0.10. The molar ratio of Al: Fe removed by this
557 fraction ranged from 15:1 to 47:1 (Figure 10). In the hydroxylamine extraction, the total Fe
558 averaged 0.017 $mg\ g^{-1}$ soil ($\sigma = 0.007$) while the concentration of aluminum extracted ranged
559 from 0.054 to 0.27 . This is once again greater than the concentration of iron extracted by the
560 extraction targeting SRO metal oxides, with an Al: Fe molar ratio ranging from just under 9:1 to
561 nearly 29:1 (Figure 10). In both extractions targeting amorphous species, a greater Al: Fe ratio
562 was seen in the 30-45 cm soils than was at the 0-15 cm depth. Finally, the amount of iron
563 removed from the soil by sodium dithionite once again outpaced the prior extractions with
564 average concentrations in each precipitation treatment group ranging from 1.78 to 5.16 mg Fe
565 g^{-1} soil. In this extraction, the molar ratio of Al: Fe pulled approaches 1:10 reflecting that there
566 were abundant crystalline Fe species at both depths (Figure 10).

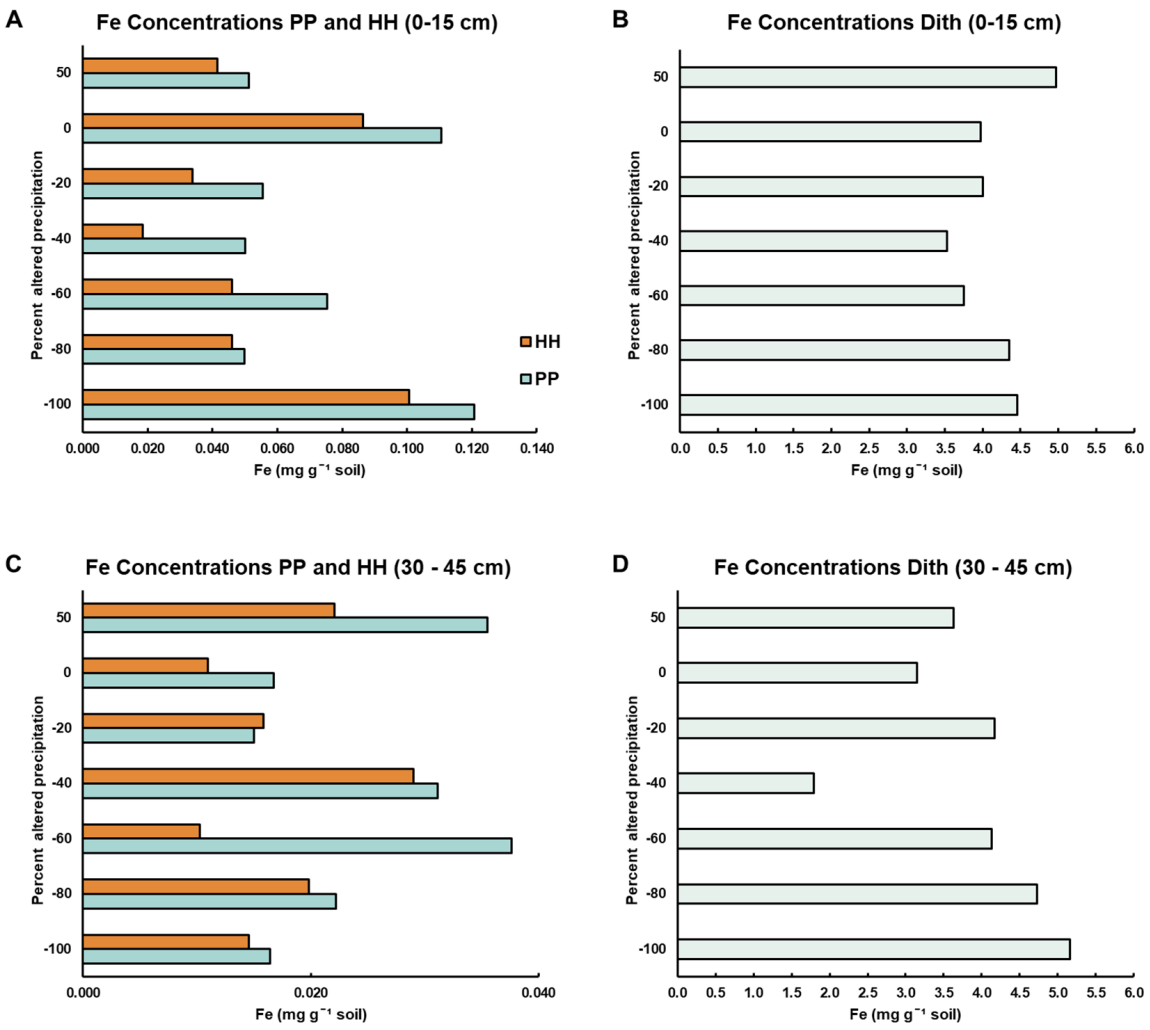

Figure 6) Graphs displaying **a, c)** the similarity in concentration of Na-pyrophosphate and hydroxylamine extractable Fe in soils of the < 53µm fraction and **b, d)** the much greater concentration of dithionite extractable Fe. Samples are grouped by precipitation treatment received on the y axis. **6 a)** and **b)** represent the soil depth of 0-15 cm, and **c, d)** show the Fe concentrations for each extraction at 30-45cm.

567

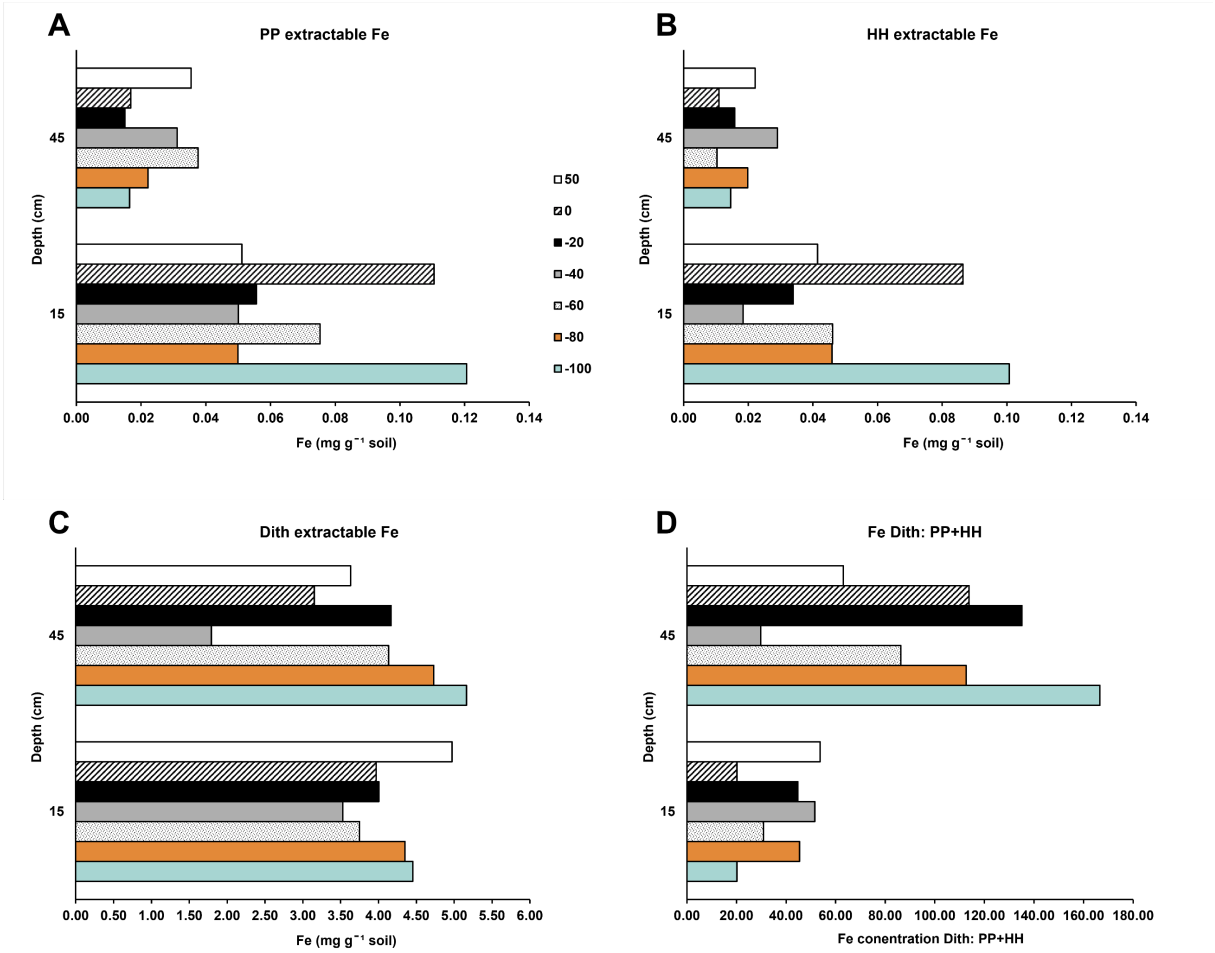

Figure 7) Soil Fe concentrations grouped by targeted extraction and depth for each treatment group **a)** Fe dissolved in Na-pyrophosphate, **b)** hydroxylamine **c)** Na-dithionite, and **d)** a ratio of Fe concentrations in the dithionite extraction to the sum of the Na-pyrophosphate and hydroxylamine extractions. Across all treatments and both depths, the majority of the Fe was of Na-dithionite-extractable, crystalline species with these Fe concentrations ranging from 20 to over 150 times that of the amorphous species Fe concentrations **(d)**.

568

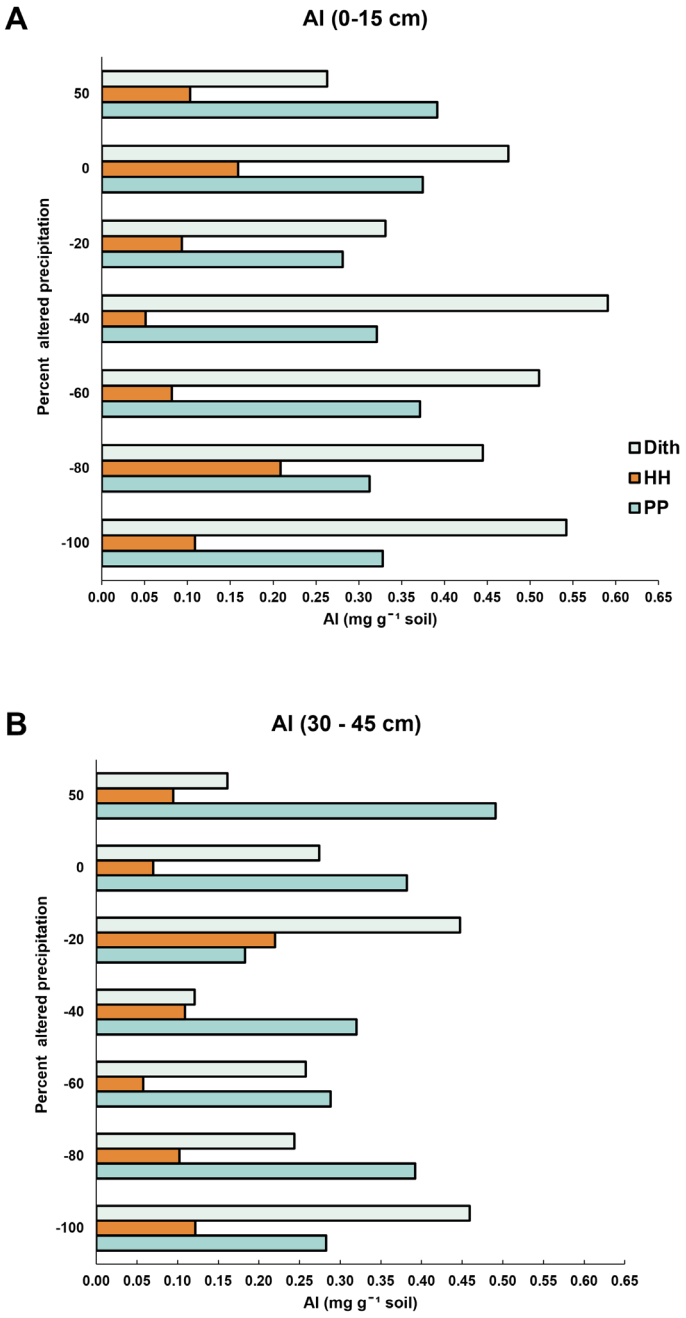

Figure 8) Al concentrations extracted from the **a)** 01-15 cm and **b)** 30-45 cm of the < 53µm fraction soils using targeted extractions at each precipitation treatment. Across all treatment groups and both depths, there was little hydroxylamine- extractable Al.

569

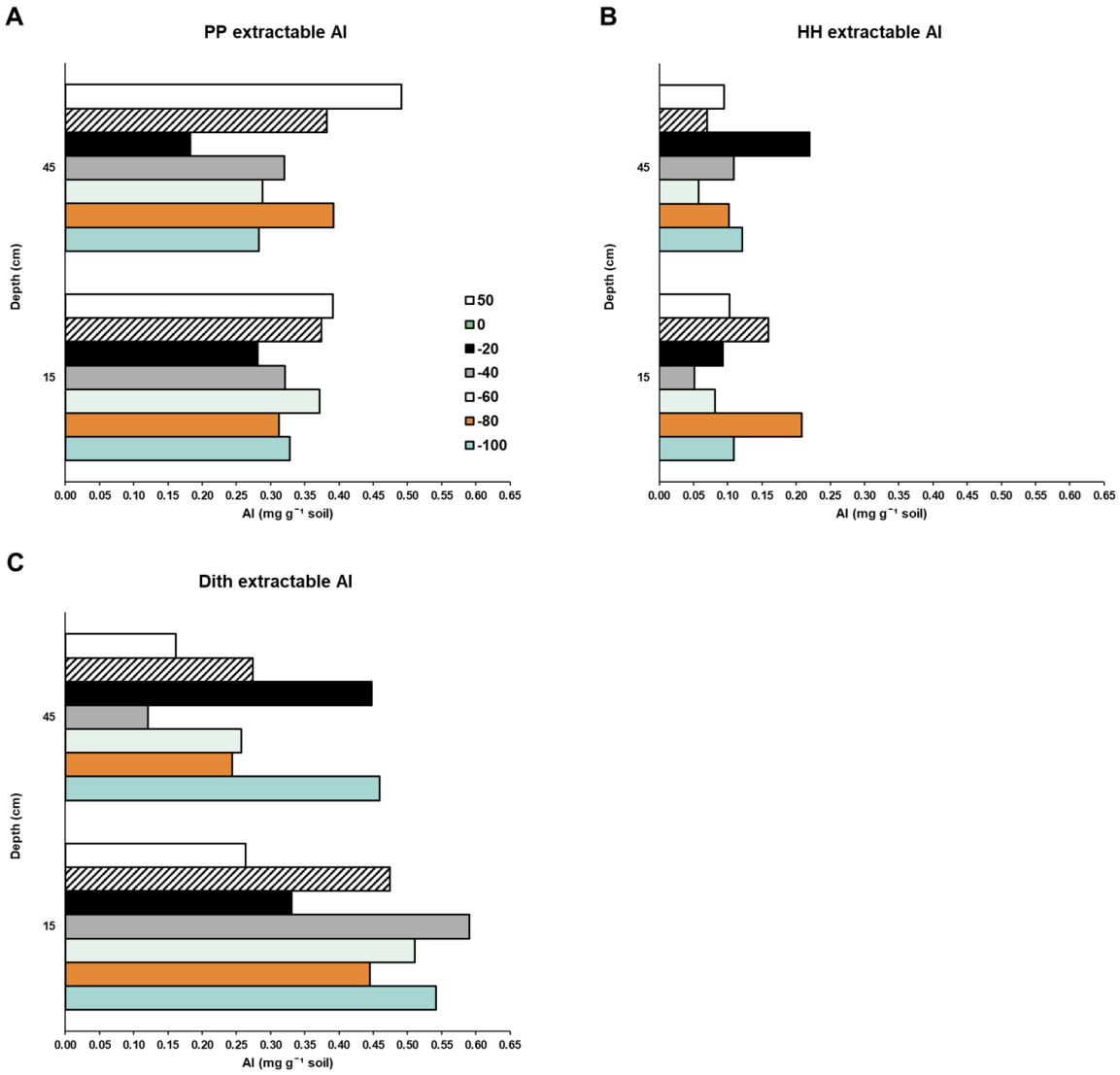

Figure 9) Average extractable Al concentrations in the < 53µm fraction soils grouped by targeted extraction and depth for each treatment group **a)** Fe extracted by Na-pyrophosphate, **b)** hydroxylamine **c)** Na-dithionite with y axis displaying soil depth and colors representing treatment groups

570

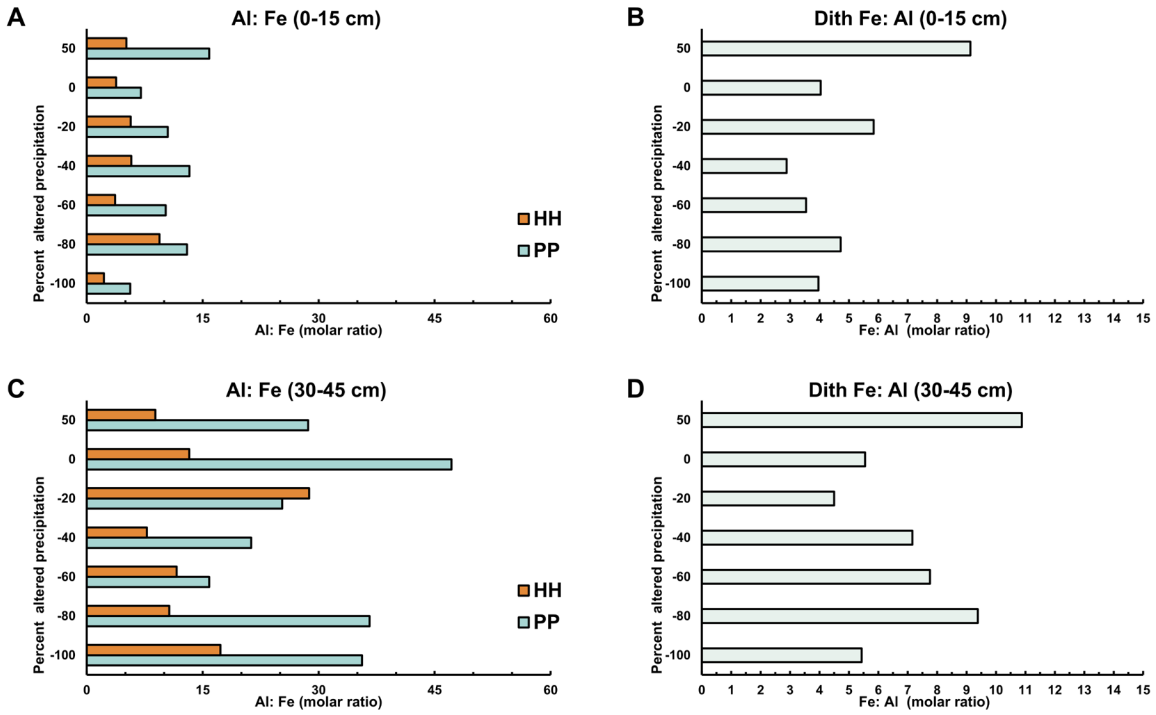

Figure 10) Molar ratios of Al : Fe concentrations extracted by PP and HH for **a)** 0-15 cm and **b)** 30-45 cm from < 53µm fraction soils. Fe: Al ratio for dithionite extraction for **c)** 0-15 cm and **d)** 30-45 cm depths. Y axis represents each precipitation treatment.

571

572 1.02.4 X-ray diffraction results

573 To determine the minerals responsible for the retention of MAOM-C following all
574 extractions, the clay mineralogy of the soil was evaluated using X-ray diffraction (Figure 11). An
575 XRD signal indicating a mixed layer clay dominated by illite was identified by the peaks at
576 10.10 Å , 5.00 Å and 3.33 Å that were broad with visible. Following the air-dried and glycolated
577 treatments, there is a peak shift from 14 Å to 16.62 Å which is characteristic of a mixed layer

clay containing smectite. An increase in peaks within the 14-18 Å following glycolation and the increase in intensity of the 10 Å peak with heating to 550 °C suggests that a vermiculite-smectite mixed layer clay may also be present as well. Finally, there is also kaolinite present as seen by the peaks at 7.16 and 3.57 Å and heat treatment causing the peak at around 7 Å to collapse.

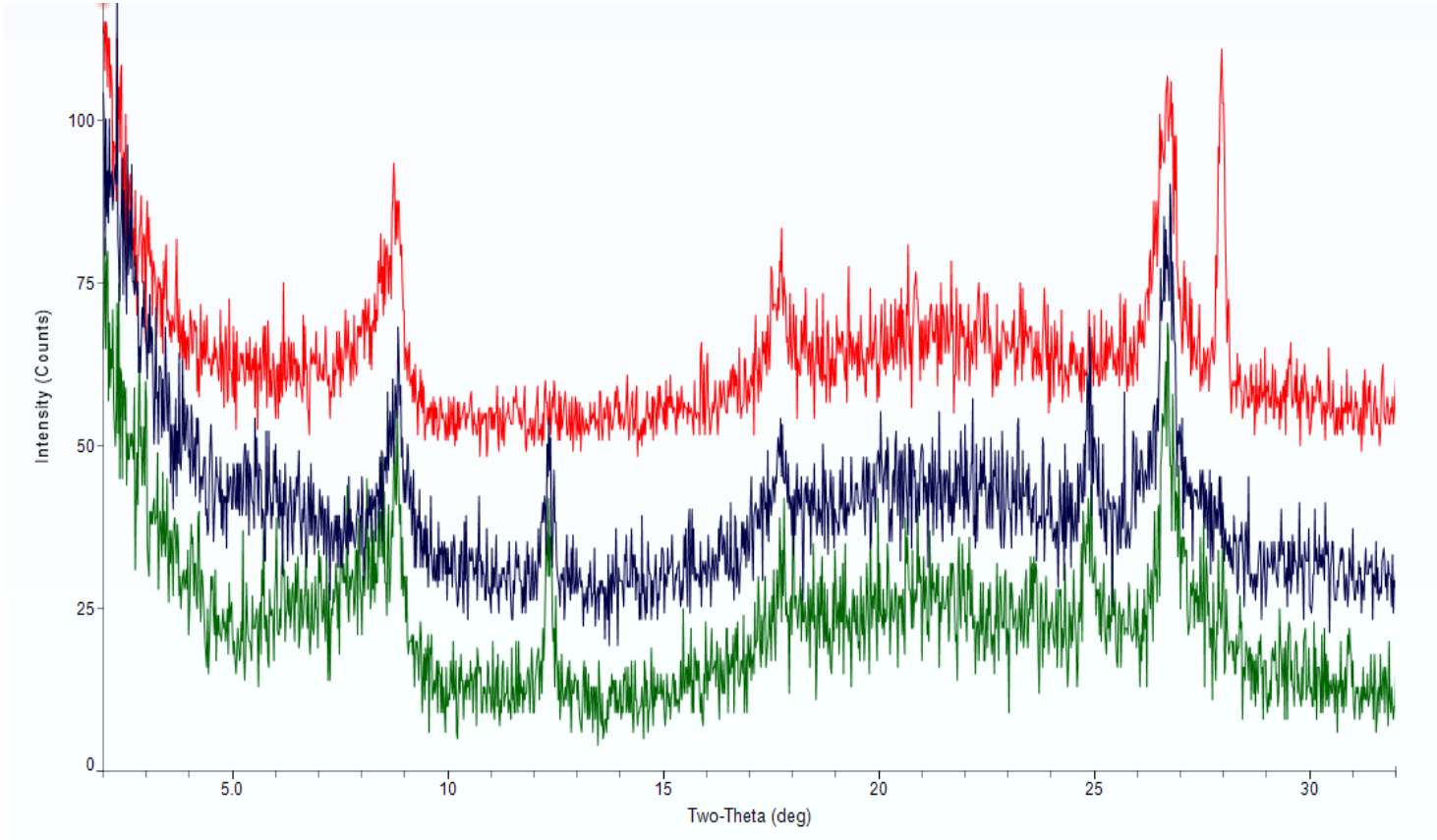

Figure 11) Fe concentrations extracted from 30-45 cm soils using targeted extractions at each precipitation treatment. Spectra were each generated following a series of treatments commonly used to distinguish between phyllosilicate clays air-dries (green), glycolation for inflating interlayers of 2:1 clays (blue), and heat treated at 550˚C (red).

582

1.03 Discussion

1.03.1 Whole soil TC and TOC

While no statistically significant trend for TC versus precipitation was identified, the variance in TC in the 30-45 cm samples especially can be explained by comparing these values to the TOC for the same samples. The lower TOC values in the 30-45 cm depth soils than the surface samples (0-15 cm) indicate that a considerable amount of inorganic carbon was removed by the HCl treatments. As expected, there are greater TOC values in surface soils where there are abundant sources for the OM from litter to roots and associated microbial communities and lower in greater soil depths with higher sand content and abundant inorganic carbon likely in the form of pedogenic carbonates.

There are several variables that likely led to the large spread of TC and TOC values seen within samples of the same precipitation treatment. One possibility is that the timescale of the experiment was shorter than needed to observe changes in SOC content induced by controlling precipitation. Castillioni et al. (2020) previously reported that the extreme lowering of precipitation inputs for the duration of the DroughtNet experiment at KAEFS led to a decrease in C_4 species and an increase in a more drought-resistant C_3 species. The variation seen in TOC values between plots of the same precipitation treatment could be a factor of both changes in fresh OM inputs and microbial community shifts associated with the transition from dominance of one plant species to another. Additionally, the sensitivity of microbial communities to extended wetting and drying periods have been shown to be variable across different soil depths and disturbance levels (Brangarí, et al., 2022). In addition to changes in the dominating plant

605 species, an increase in precipitation was found to increase aboveground net primary productivity
606 (ANPP) in the KAEFS DroughtNet experiment (Castilloni et al, 2020). While root density and
607 other measures to quantify belowground NPP were not assessed under drought manipulation
608 conditions, root density has been found to increase with increasing temperature at KAEFS (Wan
609 et al., 2005). Furthermore, this study reported an increase in soil respiration over the duration of
610 the warming experiment. This increase was attributed to the allocation of C toward building roots
611 biomass and, as a result, increasing root respiration with enhanced temperatures (Wan, 2005).
612 While soil moisture plays a significant role in C mineralization and storage dynamics, it is likely
613 that within the drought manipulation sites at KAEFS, below ground C increases with decreasing
614 precipitation due to a shift toward below ground biomass as seen under increasing temperature.
615 However, changes in SOM inputs and incorporation into different soil fractions may be irregular
616 as the plant community, energy allocation of the plants, and microbial response varies. Thus,
617 while the plant community was impacted by the controlled precipitation conditions in this time
618 frame and increasing temperatures have been shown to enhance root respiration, a response to
619 drought may not be reflected in SOC storage in a short timeframe.

620 Many previous studies have recorded an array of SOC responses to treatments over
621 different timescales with varying conclusions. While some studies resulted in measurable
622 changes in C concentrations in one pool of SOM such as POM, it may not be observed in the
623 whole soil TOC or vice versa. The degree to which a pool's turnover time and other inherent
624 properties impact its response to treatment over a given time frame must be called into question.
625 For instance, although MAOM is considered the more stable C fraction found in the soil with
626 turnover times up to a millennial scale, alterations to the soil through varying treatments like
627 fertilization methods, farming practices, or precipitation have resulted in changes in MAOM

carbon content. These responses, however, have been dependent upon the type of treatment, the soil mineralogy, and the timescale of the experiment as well as several other factors. In one evaluation of long-term field experiments of at least 20 years evaluating changes in soil C fractions treated with different fertilizers and subjected to crop rotation, changes in total SOC and MAOM-C concentrations over this time frame occurred but were small and largely controlled by soil texture (Just et al., 2023). Still, using the soil texture, below ground OC inputs, and organic fertilizer inputs from each study site, a predictive model for MAOM-C was created, and it was found that a threshold POM-C/MAOM-C ratio served as a predictor for MAOM-C saturation (Just et al., 2023). While the variation in climate and soil texture elicited different responses in terms of C content in POM and MAOM, the timescale of each study was not cited as a likely limiting factor for the lack of significant changes in C content in response to fertilization treatments (Just et al., 2023). Another study conducted by Mayer (2023) evaluating the impacts of mineral versus organic fertilization on SOC over 36 years found that the MAOM-C fractions of less than 63 μm, which were further divided into silt and clay, showed no difference in C content between treatments groups. Mayer (2023) concluded that either the timescale was insufficient or the MAOM fraction was already completely saturated with carbon. Additionally, it was determined that the sites containing more 2:1 clay species shared a positive correlation with MAOM-C concentrations. Despite these experiments being decades long, MAOM-C was hardly responsive to treatments in some cases, and texture exerted greater control.

Alternatively, a metanalysis of 148 drought manipulation studies across natural ecosystems around the world by Deng (2021) resulted in conclusions regarding the impact of drought on dissolved organic carbon content. These studies were shorter than those evaluating

fertilization, between 1 and 13 years. In grasslands specifically, it was found that whole soil OC decreased by 8.7% while DOC increased drastically, by 91.4%, along with microbial CO_2 (19.9%), but total soil respiration remained about the same. The proposed mechanism based on these results described the decrease in total biomass production due to drought leading to a lowering of total litter decomposition despite increased microbial respiration. The increased DOC was ascribed to either the lack of precipitation leading to decreased leaching down the soil profile or an increase in root exudates as the grassland plants shift toward prioritizing belowground biomass. While this review did not look at changes in POM or MAOM pools specifically, it did show that drought can have an impact on SOC over just a few years.

1.03.2 Targeted extractions

In each plot, the concentration of carbon remaining was much lower than the initial concentration prior to the targeted extractions. This was expected but still confirmed that Fe and Al mineral species were present and binding OC. However, there was not a definitive relationship between precipitation and to what form of iron or aluminum species (amorphous or crystalline) much of the C was bound. The variation within plots of the same treatment left a pattern difficult to discern. However, while precipitation may not predictably influence C storage in this experiment, valuable observations may still be made about what mineral species hold OC in this system.

In general, the concentration of C decreased after the removal of organometallic associations suggesting that these loose associations are highly concentrated in C when compared to the overall C concentration in the less than 53 μm fraction for each respective plot.

In the few instances where the initial < 53 μm C concentration is lower than the concentration following the first extraction, such as in two plots at 0-15 cm depth (at -100% natural precipitation and -60%) as well as in one at 30-45 cm depth (-20% precipitation), there was likely a lower concentration of C bound to free metal species relative to the amount of iron or aluminum pulled from this first extraction (Figures 4, 5). Though there was not a clear relationship between the carbon concentrations and precipitation alone, the implications of the changing C concentrations following each targeted extraction may be better understood when considered within the context of iron and aluminum concentrations following each extraction.

In soils from depths of 0-15 cm and 30-45 cm, the concentration of Fe pulled by the sodium dithionite extraction is 100 times greater than that which was pulled by the first two extractions which targeted more amorphous iron species (Figure 7). This either suggests that the first two extractions did not fully remove the amorphous species or that this soil is abundant in crystalline iron oxides that are not preferentially binding OM. By considering the overall decrease in C concentrations following the first two extractions in all precipitation treatments and across both depths compared to the C concentration of the whole < 53 μm soil fractions, it is apparent that a significant amount of C was removed by extractions targeting free Fe and Al and SRO species. Additionally, the change in C concentration following the first two extractions was within the same magnitude as the change following the Na-dithionite extraction despite the much higher Fe concentration in the Na-dithionite extraction (Figures 4, 5). From this we may conclude that there is indeed a greater propensity for C to bind to the poorly crystalline species across the board even when there is a high abundance of crystalline species. Such a mechanism is supported by the higher SSA available to C for binding with SRO iron oxides as opposed to the larger, less reducible hematite crystals which are derived here from red bed sandstones. In

fact, the lower surface area-to-volume ratio of hematite compared to SRO species has been previously associated with resistance to Fe reduction in hydric soils with red bed parent materials (Mack et al., 2019).

Another consideration is the role of aluminum species which may also bind OC. In the 30-45cm depth samples evaluated, there was more Al $mg\ g^{-1}$ soil extracted by sodium pyrophosphate than there was by the hydroxylamine solution apart from the -20% natural precipitation treatment group (Figure 8). In the 0-15 cm depth samples, there was a greater concentration of Na-pyrophosphate- extractable Al in all treatment groups. This points toward much of the Al being present in the form of free organometallic associations rather than SRO species. Notably, these concentrations were in a comparable range to the concentration of Al extracted by sodium dithionite, contrary to what is seen with Fe. When comparing the amount of Al pulled by each targeted extraction to iron, there is much more Al pulled than there is Fe by the first two extractions with the ratio of Al to Fe being highest in the pyrophosphate extraction for both depths (Figure 10). Next, the total concentration of each of both Al and Fe are generally lowest in the hydroxylamine extractions. This should be considered with the similarities in concentrations of C prior to and following the removal of SRO species. On one hand, little to no change in soil C concentration following the removal of SRO Fe and Al oxides along with the lower Al and Fe concentrations could suggest that the solution did not adequately extract the targeted minerals. More likely is the case that some SRO species were dissolved by the prior extraction. While a less powerful oxidant, some studies have found overlap in the amorphous species extracted by sodium pyrophosphate and hydroxylamine (Li et al., 2023; Slotznick et al, 2019). Thus, the SRO fraction could be slightly underrepresented. However, the concentrations of Fe and Al extracted by Na-pyrophosphate and hydroxylamine were within the same order of

719 magnitude for each respective element. This supports our conclusion that there were still Fe and
720 Al SRO minerals present that were not as easily reduced as species drawn out by sodium
721 pyrophosphate. Therefore, much of the SRO pool must be correctly identified. Additionally,
722 when evaluating the change in C concentration following the hydroxylamine extraction, we are
723 not directly quantifying the amount of C extracted by the hydroxylamine. As a result, little to no
724 change in C concentration could also indicate that the concentration of C bound to SRO species
725 was simply a similar C concentration to that of the soil prior to extraction of the SRO pool,
726 resulting in a C concentration value that is unchanged. In conclusion, it may be likely that there
727 is a smaller pool of SRO species than there are free metal species, but the SRO minerals are able
728 bind more carbon per Fe or Al than what would be found in an organometallic association .

729 Next, the molar amount of Fe removed by sodium dithionite is greater than the amount of
730 aluminum in all precipitation treatments contrary to what is seen in the previous extractions
731 (Figures 6, 7). A general decrease in C concentrations resulting from the removal of crystalline
732 species that are now identified as primarily iron oxides was seen across all precipitation
733 treatments reflecting the impact this pool had on the overall < 53 μm fraction C concentration.
734 However, the change in C is not several orders of magnitude higher than the previous extractions
735 unlike what is seen in the Fe concentrations. Therefore, while the soil is dominated by crystalline
736 iron, not aluminum, oxides, these species do not preferentially hold much of the OC present in
737 the soil. Following all three targeted extractions, a pool with a concentration a little over half that
738 of the entire < 53 μm fraction remained. This indicates that much of the C present is bound
739 through other means not targeted by these extractions. The presence of 1:1 phyllosilicate clays as
740 well as 2:1 mixed layer clays could act as adsorption sites for organic matter that were not
741 responsive to the targeted extractions (Figure 11). The concentration of C likely bound to clay

742 minerals, like the overall concentration of SOC in the <53 μm fraction, showed no clear relation
743 to the amount of precipitation received. However, it is noteworthy that 2:1 clays are responsive
744 to moisture conditions due to having a hydrated interlayer which increases the availability of OM
745 binding sites. This moisture-dependent OM adsorption may not be reflected in this experiment
746 due to the variable carbon content found between plots that received the same precipitation
747 treatment or possibly due to the timescale of the simulated drought. However, it is of note that
748 the total organic carbon present in the less than 53 μm soil fraction is almost equally divided
749 between Fe and Al bound species and what is most likely the remaining clay minerals. With most
750 of the MAOM-C held by either clays or reactive, poorly crystalline species, there is potential for
751 an environment where long term MAOM stability is threatened by drought or frequent flooding.

752

753 1.04 Conclusions

754 Although no clear correlation was found between drought treatments and either whole
755 soil TOC or C content within the < 53 μm MAOM soil fraction, the distribution of OC within the
756 MAOM was successfully analyzed. It was found that in both surface (0-15 cm) and deep soil
757 (30-45 cm), the concentration of C was lower following the removal of C bound to amorphous
758 then crystalline Fe and Al species. However, a soil C concentration of at least half of the
759 concentration of the whole < 53 μm fraction remained following the sequential extractions.
760 Through X-ray diffraction, we identified clay minerals that may be binding the remaining C in
761 the MAOM fraction. Within the extractions, the vast majority of the Fe was found to originate
762 from crystalline species whereas the Al was more evenly distributed between amorphous and
763 crystalline states. The small changes in C concentrations following these extractions contrasted

764 with the high dithionite-extractable Fe concentrations led us to conclude that while crystalline Fe
765 species are abundant in this soil, the more reactive and less crystalline species are protecting
766 more OC within the MAOM. With more easily reduced species and clays subjected to shrinking
767 and swelling much of the OC within the < 53 μm soil fraction, a longer-term study could
768 potentially see the impacts of precipitation on MAOM. Future directions should also quantify
769 changes in POM as previous studies have catalogued changes in the plant and microbial
770 communities during this drought experiment. The evaluation of C turnover in the face of climate
771 change is a subject in need of continual study.

ABSTRACT: CHAPTER 2

Excessive loading of sediment into waterbodies has been shown to severely diminish water quality. In Norman, Oklahoma, this issue impacts a source of drinking water for the residents, Lake Thunderbird. Here, we evaluated potential sources of soil erosion that could cause high suspended sediment within this watershed. Specifically, we conducted geochemical analysis on suspended sediment collected using a passive sediment trap deployed in Dave Blue Creek, a stream which feeds into Lake Thunderbird. We compared the suspended sediment to soil in surrounding areas that were representative of potential source groups. These source areas were ultimately grouped by land use: grasslands, tree cover, and developed land as classified by the National Land Cover Database (NLCD). We hypothesized that most of the suspended sediment in Dave Blue Creek would originate from upland urban soils. Using the Sediment Source Assessment Tool (Sed_SAT), we obtained unique geochemical fingerprints for each source group and were able to characterize changes in sediment input contributions. We successfully identified contributing sources to the suspended sediment in Dave Blue Creek based off land use. However, we found that we were unable to differentiate between bank and upland sources of the same land use. Still, clear contributions from developed land were identified across all suspend sediment samples. Additionally, we found that during the sampling periods with more precipitation and higher discharge in the stream, there was a strong grassland signature. Only in the month will little precipitation and low discharge were tree-covered land inputs detected. Overall, our results indicated that erosion control strategies in the Lake Thunderbird watershed should focus on ensuring bank stability in developed areas and mitigating run-off in grasslands.

CHAPTER 2 TRACING SOURCES OF SUSPENDED SEDIMENT IN DAVE BLUE CREEK, OKLAHOMA

2.00 Background

2.00.1 Environmental and Anthropogenic Drivers of Sediment Loading

Surface soil and stream bank erosion have the potential to detrimentally impact soil and water quality. The loss of surface soil results in the removal of organic matter, nutrients, and structural components of the soil (Fox and Papanicolau, 2008). The resulting runoff overloads nearby bodies of water with nutrients and heavy metals bound to sediment. An abundance of suspended sediment itself also negatively affects water quality by limiting oxygen diffusion and blocking sunlight which is detrimental to aquatic organisms. Combined with the nutrient loading associated with suspended sediments, the decay of these submerged plants can lead to excessive organic matter and conditions conducive to algal blooms in some lakes (Fatahi et al., 2022). A high concentration of suspended sediment can also physically obstruct the gills of aquatic life harming an aquatic ecosystem over every trophic level (Fatahi et al., 2022). While several environmental factors contribute to soil and bank erosion, anthropogenic activity is often a leading factor. The state of Oklahoma has a long history of poor land-management practices such as overgrazing and leaving barren fields after plowing which have led to soil erosion. Most notably, these practices combined with a period of drought resulted in the Dust Bowl of the 1930s. Following this period of drought, severe flooding became an issue and caused further soil erosion (Mundende, 2010). While decades of erosion mitigation strategies and conservation incentives have passed since the worst of Oklahoma's erosion problems, the state still faces

periods of drought and flooding which leads to soil erosion (Lake Thunderbird Management Plan, 2016). Human activities such as farming and now urban development both contribute to excessive sediment loads in streams, especially when erosion control strategies such as reduced tillage farming, terracing, and streambank stabilization, either through vegetation or construction, are not in place (Fox et al., 2016; Collins et al., 2012, 2017; Lake Thunderbird Management Plan, 2016). In a review paper discussing the need for further studies of upstream controls on sedimentation in Oklahoma, Fox (2015) summarizes reasons for poor response to erosion control strategies implemented in response to sediment loading. Reasons identified included control strategies failing to target important source areas, not adequately evaluating bank and channel erosion, not accounting for an abundance legacy sediment, or mitigation strategies being undermined by environmental changes (Fox et al, 2015).

2.00.2 Sediment Fingerprinting

It has been found that a unique signature related to a source environment may be used to determine the origin of sediment inputs into waterbodies (Walling, 2013). These signatures of a source environment, often referred to as fingerprints, can take the form of mineralogical properties of a source, trace element geochemistry, isotopic fractionation, or a combination of such markers (Koiter et al., 2013; Miller et al., 2015; Walling, 2013; Xiang & Liu, 2016) . The selected fingerprint must comprise of characteristics which are unreactive and therefore conserved upon transport downstream (Gellis et al., 2016; Miller et al., 2015). These fingerprints have successfully been used to identify sediment inputs based off land use (Walling et al., 1999; Bottrill et al., 2000). In systems with similar geology and soil parent materials such as the area surrounding Lake Thunderbird, trace elements and stable isotopes are suitable tools to

accomplish the identification of sites contributing to suspended sediment (Gellis et al., 2016; Walling & Collins, 2008). Often, an unmixing model with tests for tracer conservatism and other weighing factors is used to delineate sediment sources (Gellis et al., 2016; Miller et al., 2015). Here, we utilize such a model to identify sources of erosion impacting Dave Blue Creek.

2.00.3 Grouping Source Samples

While tracers may be used to identify land use categories contributing to sediment loading, erosion response strategies are often informed by whether the sediment contribution is largely due to soil erosion or bank erosion. This is because the processes behind erosion from these two sources are different. Stream bank erosion has been modeled in stages spurred by events that result in changes in the region's hydrology. This change in hydrology can be through urban development or by major storm events that eventually compromise bank stability to a breaking point and lead to sudden deposition of bank sediment into a stream (Fox et al., 2017). Additionally, it would be feasible for the geochemical fingerprints of bank and surface soil to be different due to the change in soil characteristics. The exposed bank soils that could contribute to erosion extend the depth of the bank and multiple soil horizons. Often, differences in bank and surface sources are characterized by using stable isotopes such as those of carbon or nitrogen or by plant biomarkers (Blake et al., 2018; Fox et al., 2008; Guzman et al., 2013; Miller et al., 2014). Anthropogenically introduced tracers such as fertilizer and pesticide derivatives as well as heavy metals have also been used to distinguish between upland sources and channels in addition to land use (Miller et al., 2014; Shajib et al., 2020). Other tracers like fallout radio nuclides for determining the time of burial or quantifying erosion have also been used to distinguish between surface and channel sources (Guzman et al., 2013).

862

863 2.00.4 Passive Sediment Trap

864 A Passive sediment trap was designed by Phillips (2000) as a cost-effective way to collect
865 time integrated suspended sediment samples. This design allows for both the adjustment in
866 sediment trap height for changes in water levels as well as the ability to collect samples at a
867 chosen interval such as following storm events or over a known period of time, and the small
868 inlet allows for fine sediment to be captured that is representative of the suspended sediment in
869 the surrounding environment with minimal alterations due to preferential flow (Perks et al.,
870 2014; Phillips et al., 2000).

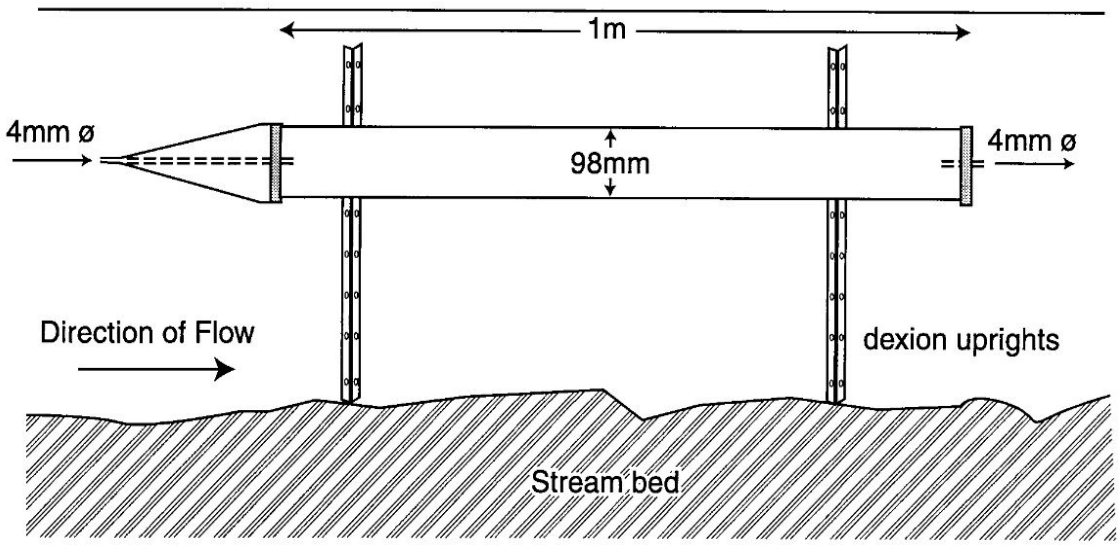

Figure 12) Schematic of suspended sediment trap design (Phillips et al., 2000)

871

872

2.00.5 Research Scope

This project serves the purpose of evaluating potential sources of sediment that contribute to the poor water quality in Lake Thunderbird, Oklahoma which serves as drinking water for the citizens of the city of Norman, OK. Lake Thunderbird has repeatedly failed to meet water quality standards for nutrients and sediment. In recent years, the City of Norman's Lake Thunderbird Compliance and Monitoring Plan established Presumptive Best Management Practices (BMPs) and Total Maximum Daily Loads (TMDLs) for "key sub-watersheds" of greatest concern within the city limits one of which was Dave Blue Creek (City of Norman, OK, 2016). In 2023, the Storm Water Quality division of the City of Norman reported that the Lower Dave Blue Creek monitoring station was found to exceed acceptable levels of total suspended solids (TSS), likely due to changes in development and land use (City of Norman, OK, 2023).

In this study, an unmixing model is applied to characterize sources of sediment and to investigate the relative proportions of these sources contributing to the sediment load captured by a passive sediment trap placed downstream of the source site. We hypothesize that through the utilization of conservative tracers (heavy metals, rare earth elements, and other geochemical tracers) we can identify primary sediment sources at a fine, sub-watershed scale.

2.01 Methods

2.01.1 Field Site

The area of study comprised of a portion of Dave Blue Creek approximately 2.5 miles long as well as the land immediately bordering this section of the stream for collecting soil from likely sediment source areas (Figure 13). Grouping potential sources of sediment into a body of

water by their geological unit or land use types are common spatially focused approaches used for sediment fingerprinting studies (Walling et al., 1999; Bottrill et al., 2000). In our study, representative source sites were selected using the National Land Cover Database (NLCD). These sites were then categorized as grasslands, tree cover, and developed land. At this scale, land use would exert greater control on sediment fingerprints than another spatial factor like the geologic unit or type of soil. Notably, the grassland and developed study areas are both dominated by the same soil series complex of Grainola, Ironmound, and Kingfisher (Table 1). Each land use was further divided between surface soil sources and bank sources for sampling.

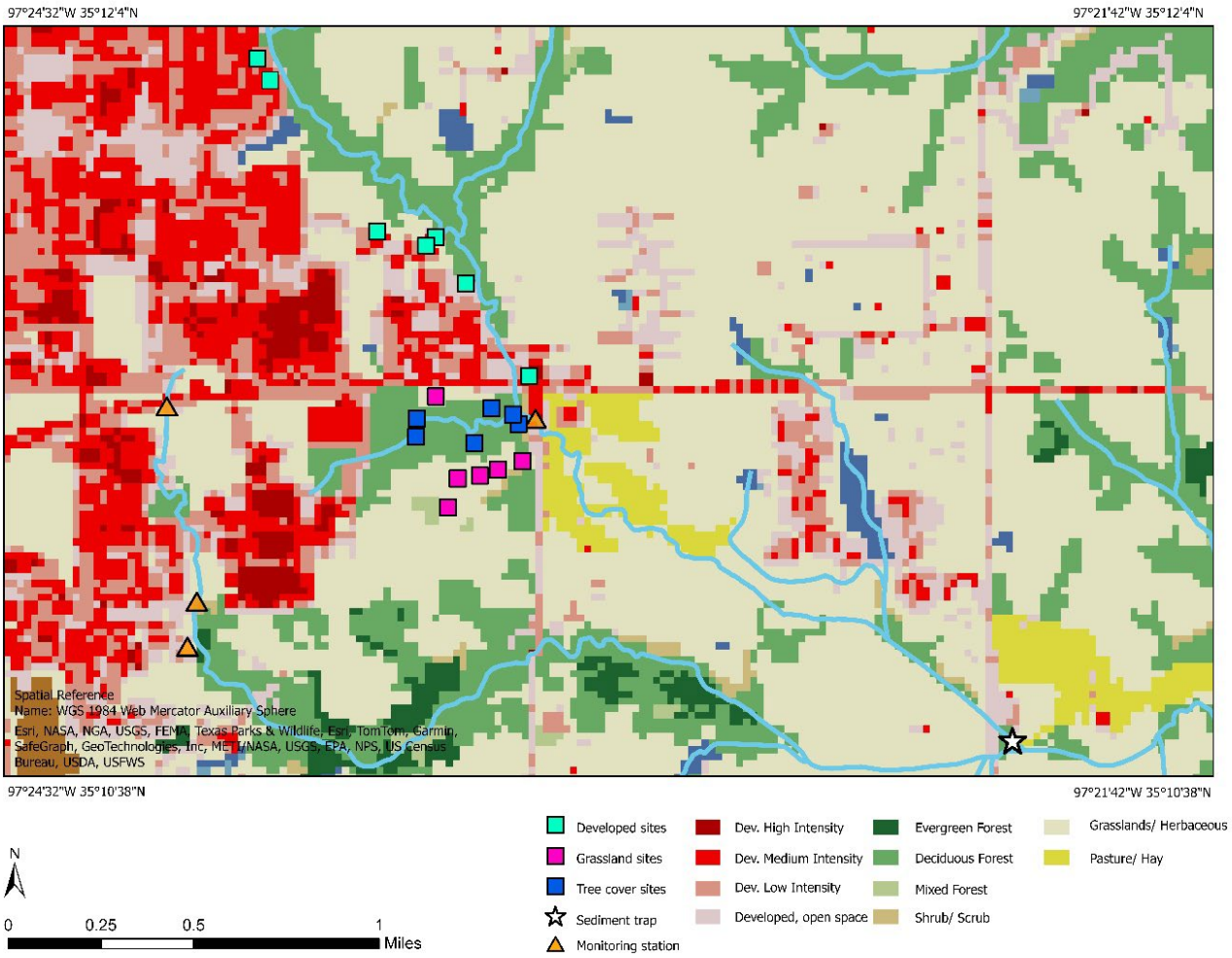

904

905 **Figure 13)** Sampling sites along Dave Blue Creek, Norman, OK. Land cover layer from the

906 National Landcover Database (NLCD) 2023.

907

908

909 **Table 1)** Description of soils present in study area grouped by land use (https://casoilresource.lawr.ucdavis.edu/gmap)

Landcover	Series	Estimated percent by area	Taxonomic Class	Soil Web Description
Grassland	Grainola -Ironmound complex	39	Gainola: Fine, mixed, active, thermic Udertic Haplustalfs	Moderately deep, well drained soils that formed in material weathered from shale of Permian age. These soils are on summits and backslopes of low hills in the Central Rolling Red Prairies
			Ironmound: Loamy, mixed, active, thermic, shallow Udic Haplustepts	Shallow, well drained soils that formed in material weathered from sandstone, or sandstone interbedded with siltstone or shale, of Permian age. These soils are on crests and side slopes of low hills in the Central Rolling Red Prairies
	Kingfisher-Ironmound complex	33	Fine-silty, mixed, active, thermic Udic Argiustolls	Moderately deep, well drained soils that formed in loamy material weathered from silty shale red beds of Permian age. These soils are on alluvial plains in the Central Rolling Red Prairies
	Renfrow	27	Fine, mixed, superactive, thermic Udertic Paleustolls	Very deep well drained soils that formed in material weathered from clayey shale of Permian age. These soils are on summits and backslopes of low hills in the Central Rolling Red Prairies
	Norge	1	Fine-silty, mixed, active, thermic Udic Paleustolls	Deep, well drained, moderately slowly permeable upland soils that formed in loamy alluvium of Pleistocene age. These nearly level to sloping soils occur on flats and upper side slopes of upland terraces
Tree Cover	Norge	60		
	Ashport	16	Fine-silty, mixed, superactive, thermic Fluventic Haplustolls	Very deep, well drained soils that formed in loamy alluvium of Holocene age. These soils are on flood plains along small streams in the Central Rolling Red Prairies
	Grainola	8		
	Ironmound	7		
	Pulaski	5	Coarse-loamy, mixed, superactive, nonacid, thermic Udic Ustifluvents	Very deep, well drained, moderately rapidly permeable flood plain soils that formed in loamy alluvial sediments of Holocene age. These nearly level to very gently sloping flood plain soils are on small tributaries
	Slughterville	4	Coarse-loamy, mixed, superactive, thermic Udic Haplustolls	Very deep, well drained, moderately rapidly permeable soils that formed in material weathered from loamy and sandy alluvial and eolian sediments, of Pleistocene age. These very gently sloping to steep soils occur on treads and risers of stream terraces, in the Central Rolling Red Prairies
Developed	Grainola	65		
	Ironmound	15		
	Kingfisher	8		
	Renfrow	7		
	Norge	3		
	Ashport	2		

910

2.01.2 Sampling Methods

Surface soil samples were sampled by collecting scrapes of the top 2 cm of soil taken in a transect at each site then pooled together to account for site variability. Bank samples were taken from bottom to top on both sides of the channel at each site then composited as well, as suggested by EPA/600/R-16/210 (Gellis et al., 2016). As individual bank and surface samples at each site for each land use were pooled, the results contained n= 5-7 individual geochemical fingerprints in each source group.

A passive sampler using the design of Phillips (2000), was installed on August 31, 2023 downstream of all field sites (Figure 15). The sampler was mounted so that it was level and completely submerged, so that the sample collected was an accurate representation of the system. The contents of the sediment trap were collected in plastic containers once a month over three months on the dates 10/09/2023, 11/12/2023, and 12/14/2023, and the trap was replaced for the next collection period. This amount of time was selected to allow for adequate sediment accumulation as there were limited flow conditions for much of the study period. Stream conditions at Dave Blue Creek are actively monitored at a site downstream from the area of study. Here, water levels and discharge were lower at the time of trap installation but increased at the end of September into the beginning of October. Through the month of November, discharge was less than 10 ft^3/s. Over the three-month period, discharge peaked approximately 249 ft^3/s in early October (Figure 14).

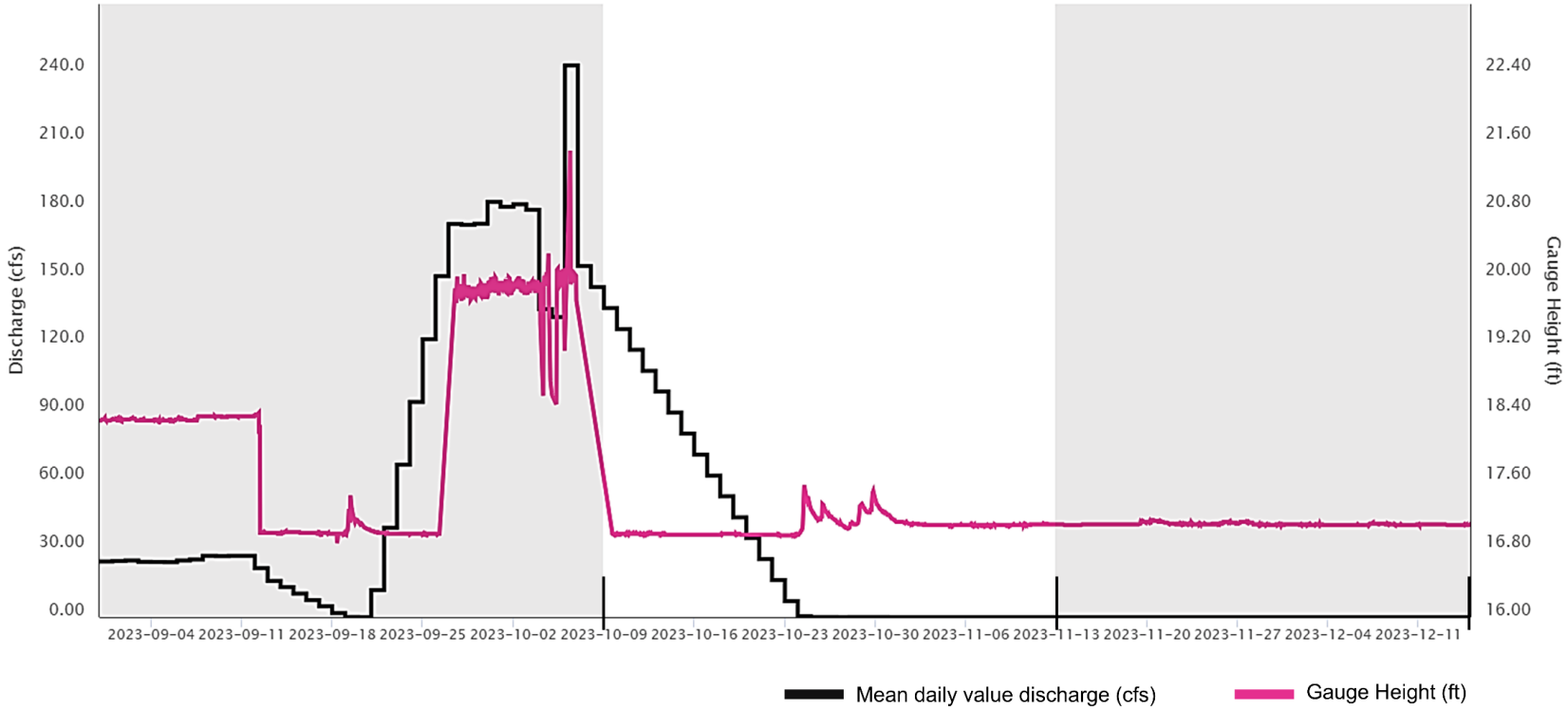

Figure 14) Hydrograph displaying discharge (cfs) and gauge height (ft) at the Upper Dave Blue Creek monitoring station over the sampling period. Each color block represents a sediment accumulation period with samples collected on 10-09-2023, 11-13-2023, and 12-14-2023. (Oklahoma Water Resource Board, 2024)

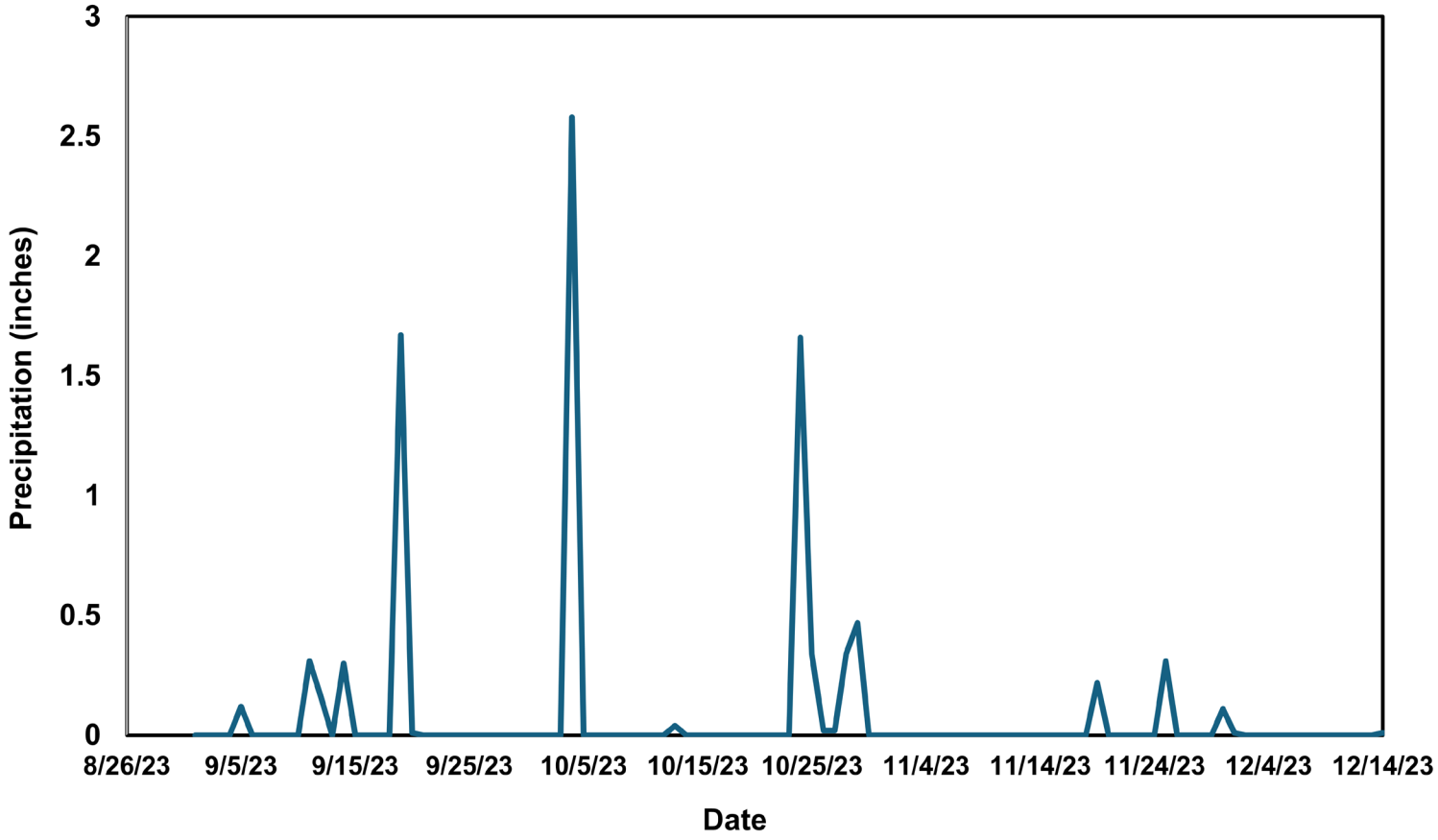

Figure 15) Precipitation events over the study period as recorded by the Norman, Oklahoma Mesonet station. Largest precipitation events over the course of the study occurred on 09/19/2023 (1.67 inches), 10/04/2023 (2.58 inches), and 10/ 24/2023 (1.66 inches) (Oklahoma Mesonet, 2025).

933

Figure 16: Passive sediment trap deployed in Dave Blue Creek

2.01.3 Sample Processing and Geochemical Analysis

The suspended sediment samples were transferred into acid-washed plastic bottles, then allowed to settle before decanting. The samples were then freeze dried, ground with a ceramic mortar and pestle, weighed, and sieved to <63 µm. The soil samples were oven-dried at 40°C, ground, and sieved to the same size fraction. (Collins et al., 2012; Gellis et al., 2016) Samples were analyzed for whole rock geochemical analysis using an Aqua regia digestion followed by ICP-MS by an outside laboratory, Australian Laboratory Services (ALS) Global.

2.01.4 Sediment Source Assessment Tool (Sed_SAT)

The results from the geochemical analysis were used to create a sediment fingerprint so thar we could identify conservative tracers and determine the origin of the sediment load captured by our trap. Here, we input our samples into the Sediment Source Assessment Tool (Sed_SAT) (https://www.usgs.gov/software/sediment-source-assessment-tool-sedsat). This unmixing model was selected for its inclusion of tests for tracer conservatism and robust error analysis in addition to an unmixing model. After evaluating if each tracer is distributed normally or requires a mathematical transformation to do so, the model identifies outliers. Two samples containing outliers, greater than N=3 standard deviations from the mean, for concentrations of Na, Ti, Nb, and V were identified and these values were excluded from future steps. Next, a Bracket Test was done to identify which tracer concentrations do not change dramatically from the source areas to the suspended sediment samples. The tracers with less than 10 percent change in concentration between the sources and the suspended sediment were identified as being conservative as shown by Equation 1 (Gellis et al., 2017).

$$\min(Y_i) - p * \min(Y_i) < xi < \max(Y_i) + p * \max(Y_i)$$

xi = suspended sediment concentration value for the given tracer

Yi = vector of all source tracer concentrations for tracer (i)

p = increase in range of the source dataset = 0.1

Equation 1: Bracket test for tracer conservatism (Gellis et al., 2017)

957

958 Of the 52 elements included in the sample geochemical fingerprint, 22 tracers were
959 flagged as nonconservative by the Bracket Test and thus eliminated. The racers identified as
960 conservative were Mg; Nb; Th; U; Lu; Yb; As; B; Ba; Ce; In; La; P; Pb; Sb; Sc; Ti; V; Zn; Dy;
961 Er; Eu; Gd; Ho; Nd; Pr; Sm; Tb; Tm. The source and suspended sediment data were then
962 evaluated by a series of multivariate tests. The purpose of these tests was to determine if the
963 transformations applied to the selected group of tracers meet the assumption of linearity
964 underlying a Forward Stepwise Linear Discriminant Function Analysis (DFA). The DFA was
965 performed to identify a profile of tracers with the greatest discriminatory power between groups.
966 Here, we selected a significance value of 0.05 for Wilks Lambda discriminatory analysis method
967 used in this step of the model. Sed_SAT also included a cross-validation approach to determine
968 the extent to which the selected tracers from the DFA would belong to its source group if its
969 origin was unknown (Gellis et al., 2017). The output of the cross-validation was used in Equation
970 2 to weigh tracers in the unmixing model based off how well each of the remaining tracers
971 correctly characterizes each source sample.

$$W_i = \frac{P_i}{P_{opt}}$$

Pi = percent of source samples classified correctly using tracer

P opt = percent of source samples classified correctly using tracer with the lowest Pi .

Equation 2: Weighting factor calculation (Gellis et al., 2017)

Finally, a mixing model utilizing these weighting factors was used for the remaining tracers. Error for this model is calculated in Sed_SAT using Equation 3. Along with Equation 3, a Monte Carlo simulation (1,000 iterations) and the results of running each tracer through the unmixing model as if it was a target sample of unknown composition comprised the thorough error analysis in the Sed_SAT toolbox. Two iterations of the model were selected to be compared, the first separating bank and upland soil samples in each land group as their own source groups, the second differentiating source groups by land use alone. The percentage source contributions from each land use were then compared to the estimated annual runoff from sites of each land use occurring at each sample across daily precipitation inputs using the EPA National Stormwater Calculator (Environmental Protection Agency, 2025). A representative sampling site of equal area was selected for each land use group to estimate the average annual runoff based off properties of the dominant soils in each site. The parameters input included water infiltration rate, soil type, hydraulic group, slope, and land cover.

2.02 Results

2.02.1 Bank versus Surface samples

We first ran an iteration of the model grouping sources in two groups, upland and bank samples. However, unique fingerprints distinguishing between these two groups could not be generated, likely due to the differences in land use and erosional history across the watershed. In the next run of the model, we defined source groups by land use and by location: upland or stream bank. The goal of grouping samples in this manner was to identify where bank stability is a primary issue versus runoff from the surface. However, this resulted in high degrees of uncertainty in the subsequent error analysis. When individual source samples were run as unknown sediment samples to verify the accuracy of the source group fingerprint, many samples were incorrectly classified (Table 2). Additionally, we found that individual sample profiles greatly varied within a single source group when faced with 6 possible source contributions (Figure 17). As a result, a second iteration of the model which classified bank and upland soils of the same land use as one source group was run. In the subsequent error analysis, the variation between samples within the same group was lower, and only the grassland samples were mostly poorly classified by the model (Table 3). Notably, the fingerprint of the grassland samples overlapped significantly with the developed land use fingerprint (Figure 18).

Table 2) Error analysis for unmixing model with upland and bank source groups. Here, "Perfectly Classified" indicates 100 percent correct source contribution was assigned to a particular sample. A sample is categorized as "Classified" if its source contribution is < 80% of the correct group, poorly is < 50%, and incorrect is 0%.

Source Type	Number Perfectly Classified	Percent Perfectly Classified	Number Classified	Percent Classified	Number Poorly Classified	Percent Poorly Classified	Number Incorrectly Classified	Percent Incorrectly Classified
TBANK	1	25	2	50	1	25	1	25
DEVBANK	3	42.86	4	57.14	2	28.57	1	14.29
GRASS	3	25	4	33.33	6	50	4	33.33
FOREST	0	0	0	0	5	55.56	2	22.22
URBAN	0	0	0	0	10	100	3	30
GBANK	2	33.33	3	50	3	50	2	33.33

1006

1007

Table 3) Error analysis for unmixing model with only land use source groups

Source Type	Number Perfectly Classified	Percent Perfectly Classified	Number Classified	Percent Classified	Number Poorly Classified	Percent Poorly Classified	Number Incorrectly Classified	Percent Incorrectly Classified
FOREST	3	25	6	50	2	16.67	0	0
URBAN	10	62.5	10	62.5	6	37.5	0	0
GRASS	1	5.88	1	5.88	12	70.59	5	29.41

1008

1009

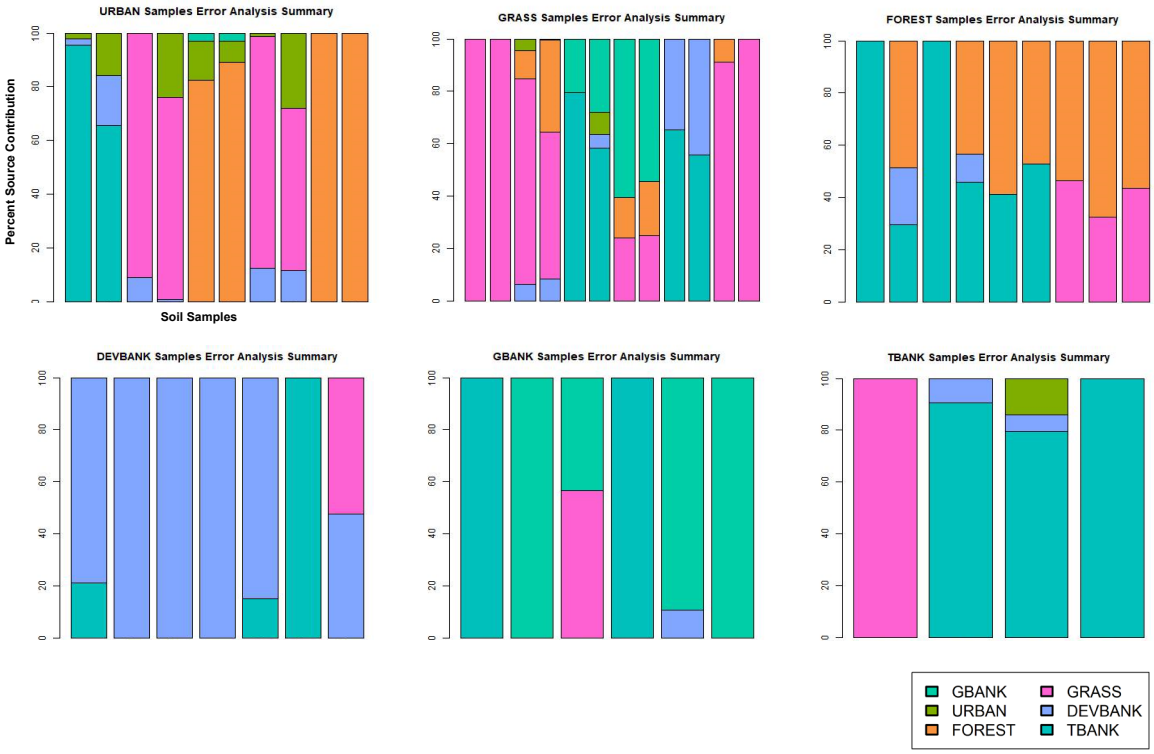

Figure 17) Error analysis summary of initial run distinguishing between upland and bank groups. Here, each source soil sample was run as if it were a collected as suspended sediment downstream to assess how accurately the fingerprint profile for a given source group identifies a sample of known origin. Here, GBANK represents the grassland bank source group, TBANK is the tree-cover bank group, and DEVBANK is developed bank group. URBAN, GRASS, and FOREST refer to their respective upland source groups.

1010

1011

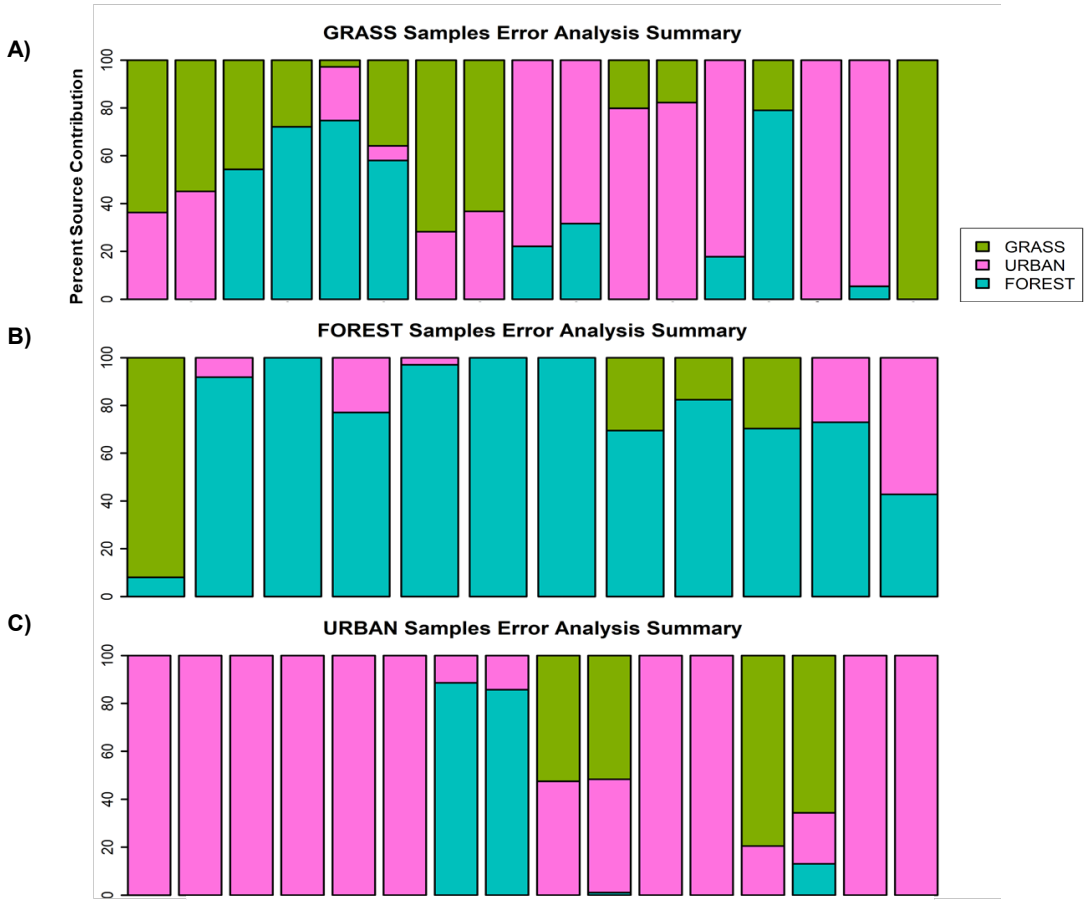

Figure 18) Error analysis summary evaluating if a soil sample of known origin may be correctly identified as belonging to its source group which here are sorted by land use only.

1012

1013

1014 2.02.2 Determined Sediment Sources

1015 The unmixing model resulted in estimated mixtures of the sources for each sediment
1016 collection period. In the run with bank and upland source groups, the suspended sediment
1017 mixtures were found to be 53.45 % developed bank origin and 46.55% upland grassland in

September; 21.13% developed bank and 78.87% upland grassland in October; and 14.09% developed bank and 85.91% upland tree cover in November (Figure 18). Despite the inclusion of 6 potential source groups, only three groups were ever identified as contributing to sediment samples. Specifically, only one group of each land use was included. However, the results when grouping sources by land use showed similar source contributions. The September sediment was determined to be 30.89 % developed sources and 69.11% grasslands, and the October sediment was found to be 52.67 % developed in origin and 47.33% grasslands. The November sediment was identified as 46.2% developed and 53.8% tree-cover sources (Figure 20). The greatest difference was between the November sample percent source contributions and likely reflected the large portion of the upland developed samples that were attributed to tree cover sources in the error analysis of source groups (Figure 18).

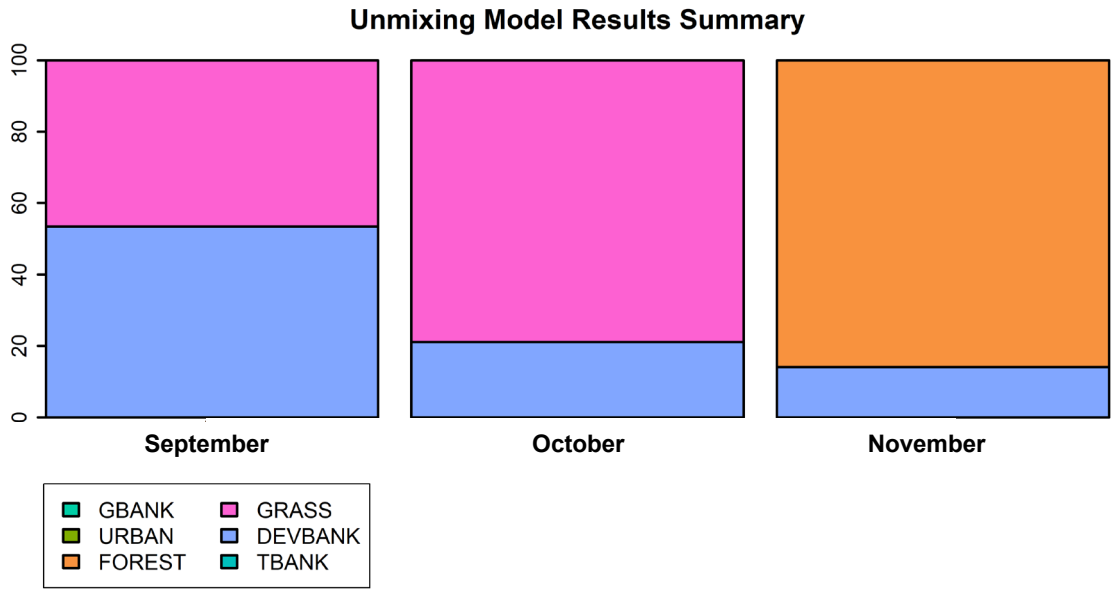

Figure 19) Unmixing model results over sampling period with bank and upland sources. The total precipitation received over each month was 2.57 inches (September), 5.47 inches (October), and 0.64 inches (November) (Oklahoma Mesonet, 2023).

1030

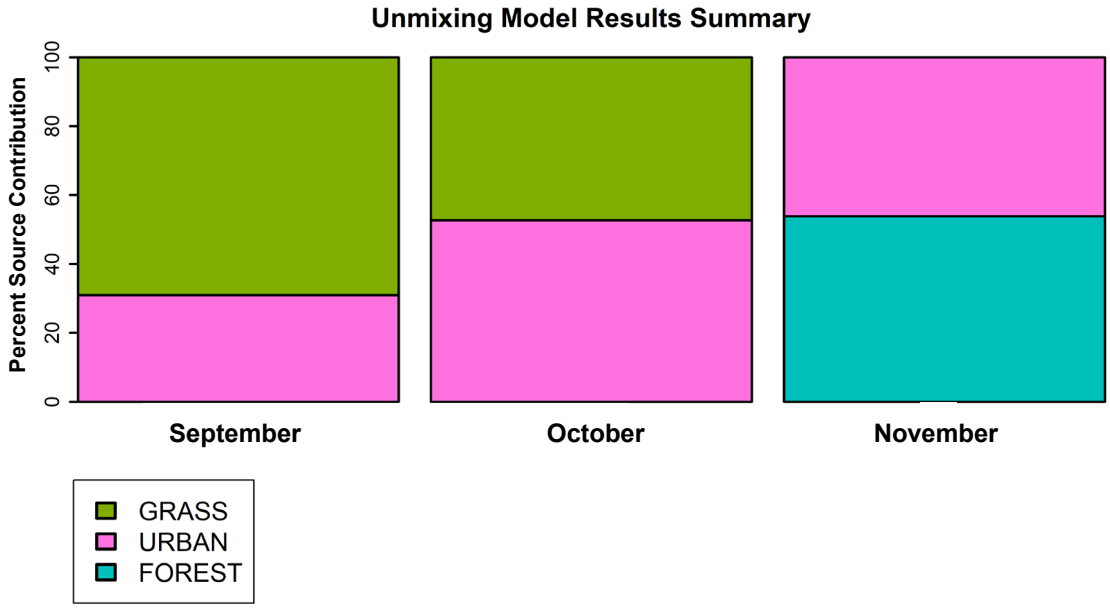

Figure 20) Unmixing model results with only land use source groups. The total precipitation received over each month was 2.57 inches (September), 5.47 inches (October), and 0.64 inches (November) (Oklahoma Mesonet, 2023).

2.02.3 Tracer by Tracer Plots

Following the Linear Discriminatory Function Analysis, a smaller list of tracers remained that would generate source group sediment fingerprints with optimum separation for each run. Grouping samples by land use only as compared land use and bank versus surface resulted in the selection of different tracers to create unique fingerprints for each source group. More tracers were required to create a unique fingerprint for upland versus bank samples of the same land use, and even then, the discriminatory power of the fingerprints was inadequate. As a result, the elements used as tracers in the first run of the model were As, Lu, Mg, Sc, Sm, Th, U, V, and Yb where Yb was utilized to classify the most samples (Table 4). On the other hand, Lu, Mg, Nb, Th, U, and Yb were deemed the best tracers for characterizing land use samples with Nb as the

strongest identifier (Table 5). Notably, there is some variation in concentrations of tracers between the sediment samples collected over different months such as an increase in As in the November samples and higher Th in the September sample (Table 6). Tracer by tracer plots were used to demonstrate how well each element concentration coincided with the overall source contribution percentages. In the run which separated upland and bank sources, the average tracer concentrations for the developed bank samples share closer values to the sediment samples for As, Lu, Sc, Sm, Th, U, V, and Yb but not for Mg which is closer to the concentration found in the surface tree cover and grassland samples (Figure 21). With samples grouped only by land use, the developed samples are closest to the suspended sediment values for Lu, Th, and Yb, but are notably lower than the other sources' Mg, U, and Yb concentrations reflecting how the U concentration in developed bank samples were higher than the developed upland samples (Figure 22). A similar pattern is seen with grassland samples where upland grasslands are of a greater Mg concentration than their bank counterparts (Figure 22). Finally, it must be noted that in some tracers, while still within the range of being classified as conservative, show an increase in concentration within the suspended sediment downstream of the sample sites (Figures 21, 22). This is especially the case for uranium, where the sediment samples from all three months had a higher U concentration than any one of the land use average samples.

Table 4) Discriminatory Function Analysis (DFA) for the sediment fingerprint of the run with land use source groups and upland versus bank designations where Wi is the tracer weighing factor applied to each tracer.

Tracer Names	Wilks lambda	F statistics overall	p value overall	F statistics diff	p value diff	Cumulative Percent Classified	Individual Percent Classified	Wi
Th	0.37	14.43	3.14E-08	14.43	3.14E-08	24.868	24.9	307.4
Mg	0.15	12.75	4.32E-13	11.49	4.99E-07	54.749	29.6	365.4
Yb	0.09	10.48	3.30E-15	6.04	2.82E-04	48.915	38.2	471.6
Sm	0.04	11.23	8.80E-20	11.10	9.44E-07	53.082	33	407.4
Lu	0.01	12.14	2.36E-24	11.33	8.59E-07	63.545	36.8	454.3
Sc	0.01	11.05	4.66E-25	3.95	5.53E-03	72.989	8.1	100
U	0.01	10.30	1.33E-25	3.67	8.54E-03	73.267	22	271.6
V	0.00	9.82	3.73E-26	3.65	8.94E-03	84.378	24.6	303.7
As	0.00	10.39	1.08E-28	7.17	1.04E-04	78.823	26.7	329.6

1059

Table 5) Discriminatory Function Analysis (DFA) for the selected tracer comprising the sediment fingerprint of the model run with land use source groups that do not differentiate between bank and surface samples.

Tracer	Wilks lambda	F statistics overall	p value overall	F statistics diff	p value diff	Cumulative Percent Classified	Individual Percent Classified	Wi
Nb	0.5985	14.09	2.08E-05	14.09	2.08E-05	62.2	62.2	205.3
U	0.4459	10.20	9.45E-07	7.01	2.35E-03	58.5	48.8	161.1
Mg	0.3563	9.00	1.64E-07	5.03	1.11E-02	62.5	36.4	120.1
Th	0.3007	8.03	7.71E-08	3.61	3.62E-02	76.1	50.2	165.7
Yb	0.1728	10.68	4.57E-11	14.06	2.52E-05	78.4	41.4	136.6
Lu	0.1240	11.34	1.78E-12	7.27	2.12E-03	85.2	30.3	100

1061

Table 6) Average tracer concentrations (ppm) for suspended sediment samples over each sampling period.

Sample Name	As	Mg	Sc	Nb	Th	U	V	Lu	Sm	Yb
September	4.9	1.53	6.3	0.35	6.7	0.87	46	0.098	4.47	0.776
October	3.6	1.18	4.7	0.29	5.4	0.67	36	0.085	3.69	0.634
November	6	1.47	3.3	0.27	2.5	0.81	31	0.138	5.11	1.145

1062

1063

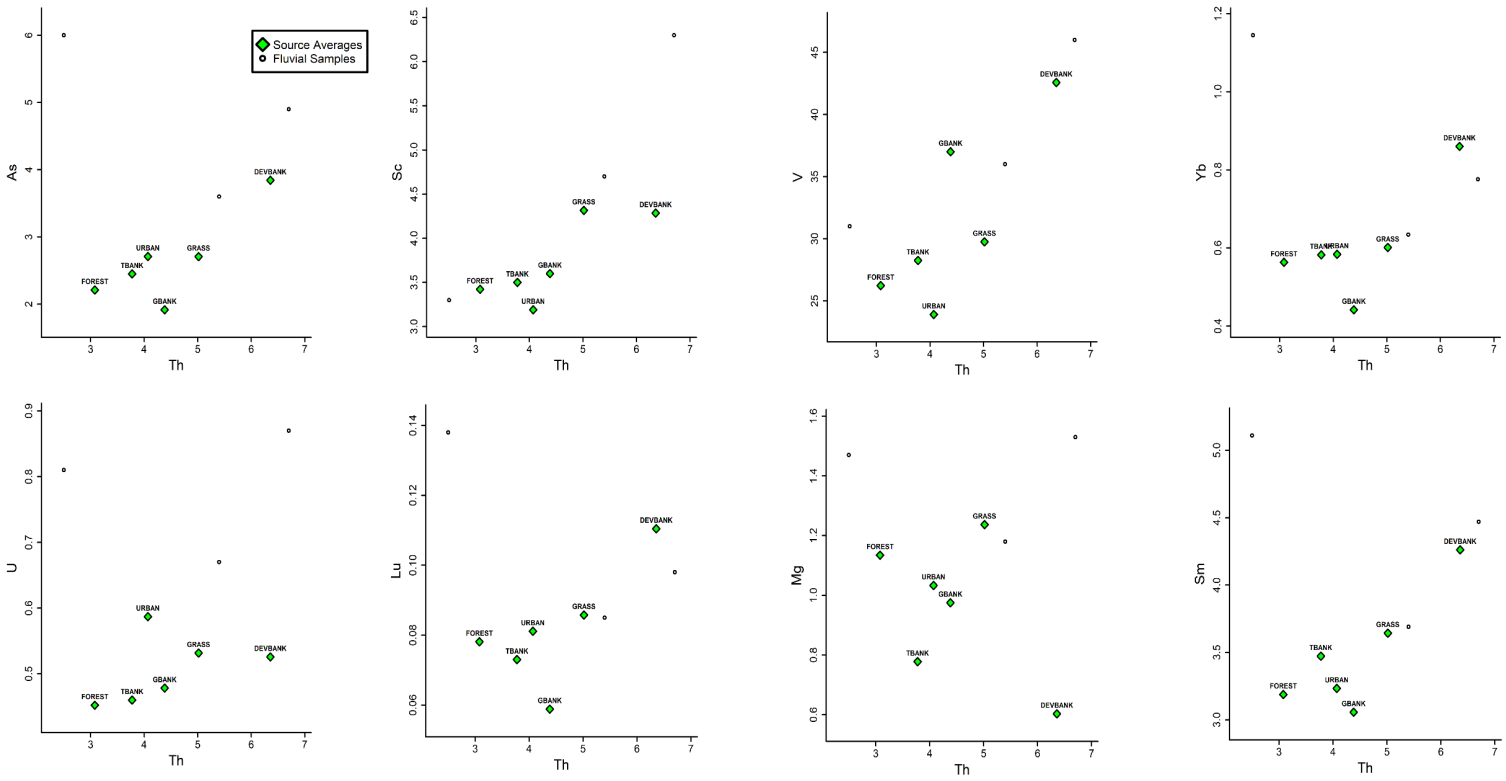

Figure 21) Average concentrations of tracers comprising the sediment fingerprint when bank and upland sources as different source groups. Tracers are plotted against the thorium concentration. Source groups are marked with diamond and suspended sediment sample concentrations are represented by circles.

1064

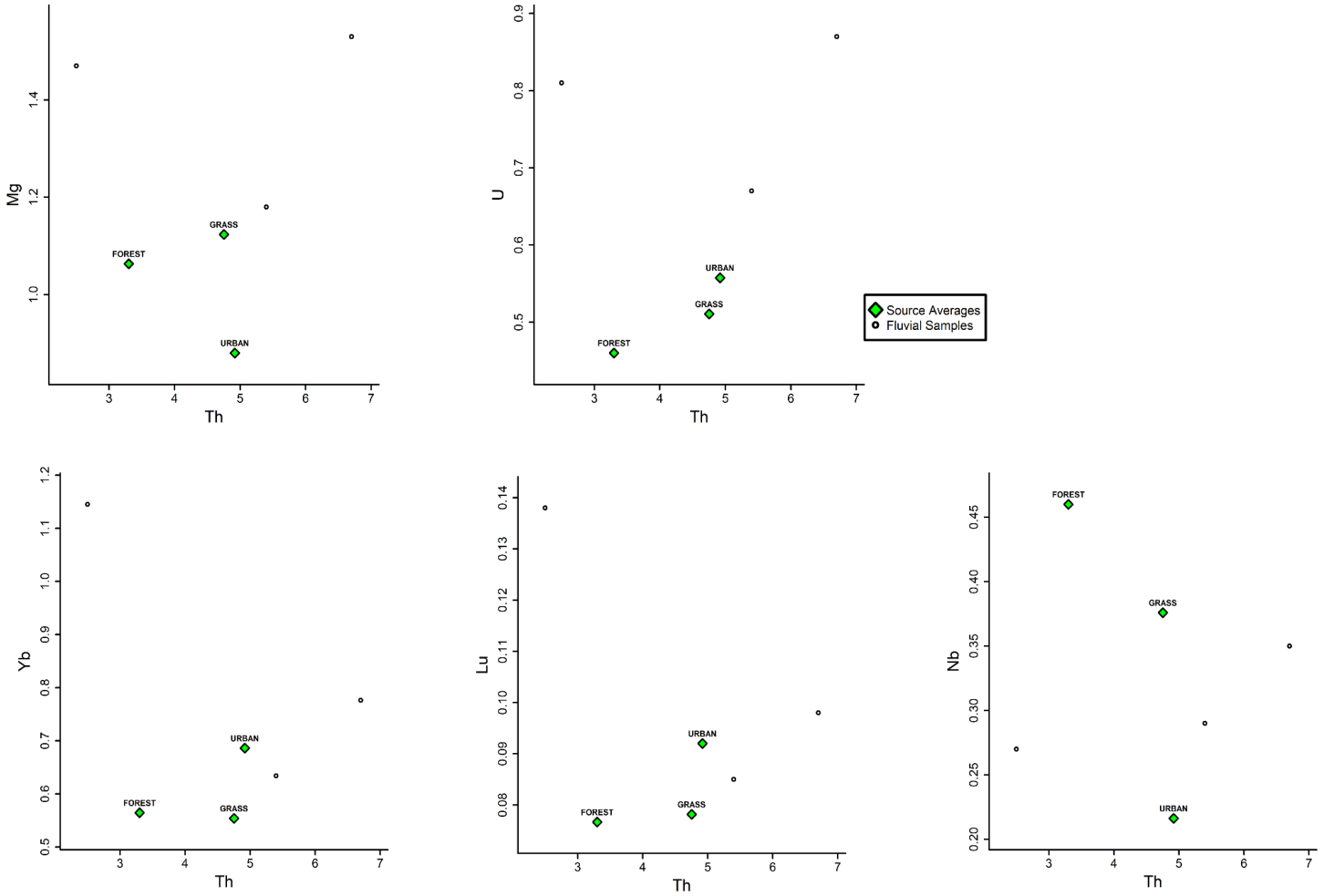

Figure 22) Average tracer concentrations for the elements comprising sediment fingerprints, plotted against Thorium, for land use groups and captured sediment samples.

1065

2.02.4 Monte-Carlo Results

A Monte-Carlo simulation was used following each model run to evaluate the uncertainty behind the model itself through repeated iterations of the run while excluding individual source samples (Figure 23). Here, the error analysis of the run with samples identified by land use only yielded identical results as the model run**.** On the other hand, there was a larger spread in land use percent contribution for each iteration of the Monte-Carlo simulation when separating source groups by both land use and upland or bank sources. This spread is seen specifically in groups that were not classified as contributing to the suspended sediment in the model results such as upland developed and tree bank samples. Thus, grouping sources by land use is a more reliable means of sediment source tracing at our study scale.

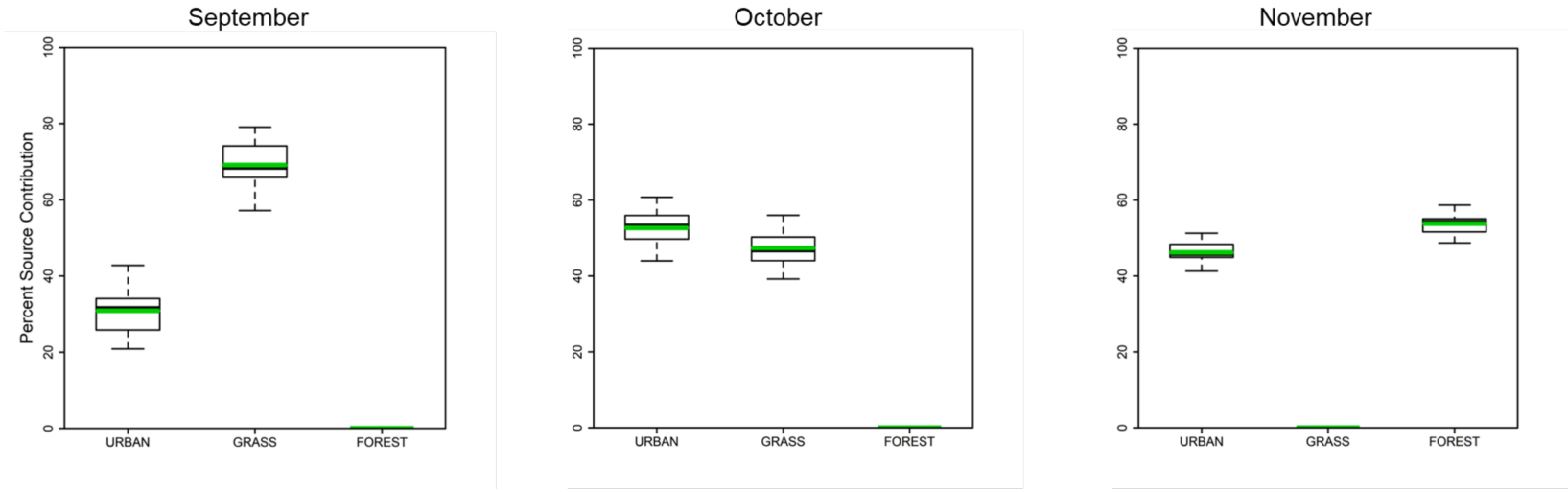

Figure 23) Box plots following Monte Carlo analysis of land use run. The green bar represents the average percent source contribution in all simulation iterations with the black bar showing the median value. The total precipitation received over each month was 2.57 inches (September), 5.47 inches (October), and 0.64 inches (November) (Oklahoma Mesonet, 2023).

1078

2.02.5 Comparison of Sediment Load to Calculated Runoff

Using the study site's average annual rainfall over the last 20 years, 33.81 inches, the EPA National Stormwater Calculator shows the site with tree cover to have the least annual runoff at only 0.55 inches or 1.6% of the annual received precipitation (Figure 24). On the other hand, the grassland site lost 5.68 inches of precipitation, 16.8% of the average annual precipitation, as runoff. Meanwhile, the developed site had an estimated 9.16 inches of runoff, 27.1% loss (Figure 24). Additionally, by plotting daily precipitation events over this timescale versus runoff, the similar higher runoff in grassland and developed land uses compared to tree cover are apparent (Figure 25).

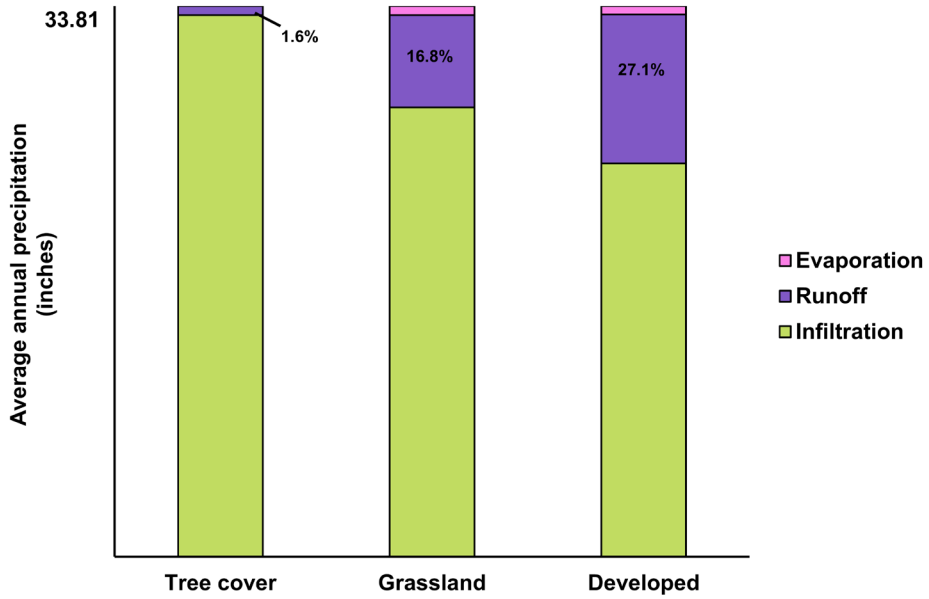

Figure 24) Proportion of average annual precipitation (inches) fated for evaporation (pink), runoff (blue), and infiltration (green) at each land use site as determined by the EPA National Stormwater Calculator (https://swcweb.epa.gov/stormwatercalculator/). 33.81 inches is equal to 100% of the average annual precipitation over the span of 20 years.

1088

1089

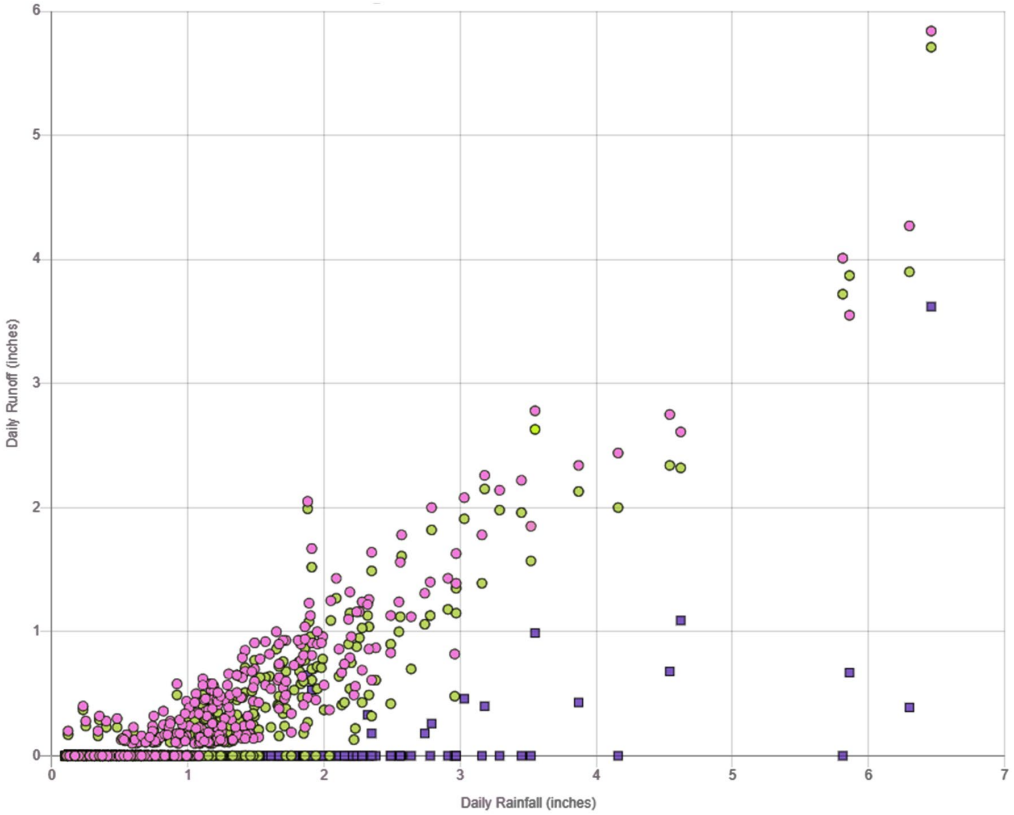

Figure 25) Average daily runoff (inches) versus local daily precipitation events (inches) over a 20-year period as estimated by the EPA National Stormwater Calculator (https://swcweb.epa.gov/stormwatercalculator/). Sites were classified by land use: developed (pink), grass cover (green), and tree cover (blue) along with physical properties of the dominant soil type at each site.

2.03 Discussion

2.03.1 Introduction

Our evaluation of contributing sources to the suspended sediment in Dave Blue Creek over our sampling period resulted in measurable inputs from each land use which changed over

time. These results are discussed here along with our error analysis tests which support such findings. These analyses consisted of a Monte-Carlo simulation as well as an evaluation of our source group fingerprints. The implications of what individual tracers were detected are then discussed. We follow this with an assessment of the similarities and differences between upland and bank samples of the same land use and conclude with future directions relating to suspended sediment source tracing and erosion mitigation.

2.03.2 Suspended Sediment Source Group Contributions

There was a shift from urban and grassland contributions in the suspended sediment collected over the months of September and October to a signature that was largely attributed to the tree-cover and developed land groups in November. This could be due to changes in precipitation seen over this period (City of Norman, 2024). September and October both had much higher precipitation totals and, as a result, greater discharge in Dave Blue Creek compared to the month of November. There was likely increased runoff from grassland and urbanized areas which lack the vegetation and bank stability associated with tree-cover during the months with more precipitation. The shift in land uses contributing to suspended sediment aligning with discharge over the monitoring period further emphasizes the importance of monitoring and addressing soil erosion especially in areas lacking tree cover. Furthermore, the developed land use signature was detected across all sampling periods suggesting that inputs due to urbanization do indeed consistently contribute to this stream's sediment load. This observation is supported by our error analysis which showed that the suspended sediment source contributions were accurately characterized by land use.

The Monte Carlo simulation showed high confidence in the results of the model run where sources were grouped by land use only (Figure 23). This suggests that grouping samples

by land use creates a strong enough signature for each source group that the removal of a random source sample does not greatly impact the estimated percent source contributions in the suspended sediment. On the other hand, there was a great amount of variance in the results of each iteration of the Monte-Carlo simulation following the unmixing model run that distinguished between upland and bank sources. This variance was a result of the similarity in signatures of the same land use. For example, the November suspended sediment forest bank and surface sample contributions were highly variable. This result supports how the similar signatures of soils within the same land use category limit confidence that forest land use signatures were exclusively from upland soils as was estimated by this iteration of the model. Meanwhile, the higher confidence when grouping sources by land use only supports that these signatures are at least correctly attributed to tree-cover sources.

2.03.3 Comparison to Runoff estimates

By evaluating the percentage runoff alone using the EPA Stormwater Calculator, a majority developed signature would be expected in the suspended sediment across all months (Figures 24, 45). This is supported in the results of the unmixing model with only land use source groups where a developed signature is seen across all three months (Figure 20). Here, the months of September and October show a split between grassland and developed sources. These months were also characterized by more intense precipitation events relative to November (Figure 15). The scale of grassland areas versus developed and tree covered sites also plays an important role in source apportionment. The immediate study site is classified as 41% grasslands, 34% developed, and 25% tree cover (Esri Sentinel-2 Land Cover Explorer, 2025). While developed areas may have greater estimated runoff, there is more grassland landcover within the Dave Blue Creek watershed. Although, there are sites of active development in the

study area which suggest that these percentages will soon change and magnify the impacts of the higher runoff from developed areas. Another consideration is how the developed signature is more likely differentiated from grasslands mainly by its bank signature which showed more accurate characterization of individual tracers (Figures 17, 18). As a result, there is some difficulty separating upland grassland and developed sediment contributions. This could lead to an underestimation of runoff from developed sites by the unmixing model which would also align with the higher percent estimated runoff calculated for developed land uses relative to grasslands.

2.03.4 Implications of Individual Source Group Contributions

The evaluation of individual source fingerprints as if they were suspended sediment samples with unknown source contributions proved to be informative especially regarding similarities in upland and bank signatures of the same land use. Samples were often classified as belonging to a source that was related to its actual source group. For instance, the surface soil for the upland grasslands was shown to have a profile primarily of upland grassland and bank grassland soil contributions. This supports the assertion that there is a signature unique to grasslands as a whole. While 55.46% of the average grassland bank sample signature is correctly designated, the second largest contributor is the tree-cover bank source group. This suggests a similarity in tracer signatures between grasslands and tree-covered stream banks but not with developed banks. This similarity also helps to explain the lack of contribution from these bank samples to the suspended sediment in the overall mixing model results in the run that differentiated between upland and bank sources. Alternatively, the absence of these two bank groups in the sediment mixtures could also reflect better bank stability within these land uses.

The forest bank samples were also mostly assigned to the correct group with only one sample misclassified as being of grassland origin. Additionally, nearly 83% of the forest upland samples were classified as either forest upland or forest bank origin. The signatures of the upland and bank soils of forests must also then be similar. Next, while the developed surface soil fingerprint lacked a clear fingerprint, the developed bank group was categorized more accurately with 42.86% of its samples showing a 100% developed bank signature (Figure 17). Most of the remaining developed bank samples were still identified as having a greater than 50% contribution of the correct source group as well. This reflects how the developed bank signature is unique as well as explains its clear contribution to all suspended sediment samples. When assessing individual tracer concentrations, the contribution of the developed bank samples is even further supported.

2.03.5 Signatures of Anthropogenic Activity

Both iterations of the model identified developed sources as a consistent input in all target samples, and the evaluation of individual sample fingerprints within this group confirmed that its fingerprint was unique from other land uses. Specifically, the developed bank samples carried a signature that strongly influenced the fingerprint of this land use group as a whole. When comparing tracer concentrations across source groups and sediment samples, the developed bank samples were highest in concentrations for Lu, Th, Yb, Sm, and V and were closest to target sediment concentrations (Figure 21). This may suggest that these tracers at high concentrations are characteristic of anthropogenic activity while the remaining tracers within the fingerprint such as Mg, As, Nb and Sc are naturally occurring. When sample sources were grouped by land use only, the concentrations in developed samples were highest and closest to

target concentrations for Lu, Th, Yb but much lower than the target samples and grasslands for Mg and Nb (Figure 22). The similarity in tracer concentrations of bank and grouped developed soils supports that the percent contribution attributed to developed soils is accurate and more likely from developed banks than upland sources.

Another consideration is the slight increase in tracer concentrations seen downstream. While the increase was still within the range of each tracer being classified as conservative, this suggests that there is an accumulation of each of these tracers downstream from the source sites. Although there could be other potential sources for these tracers not governed by land use, such as the visible litter seen upstream which comprised of metal vehicle parts, pipes, and tires, the compounding effect of these tracers is a matter of concern. The tracers evaluated include heavy metals which can pose a risk to aquatic life and water quality and rare earth elements which are likely contaminants from industrial sources. Additionally, the mechanisms of the incorporation of some of these tracers into biomass are not well understood (Shajib et al., 2020). Overall, the results of the unmixing model reflect the impact of human activity on water quality in Norman, Oklahoma with most of the sediment loading attributed to developed land.

2.03.6 Limitations

While there is indeed shift in suspended sediment composition from developed and grassland sources in September and October, to grassland and forest contributions in November it is difficult to determine whether the inputs are of bank or upland origin due to overlapping source group fingerprints. The run of the model which separately categorized bank and surface soil sources for each respective land use and the run which grouped by land use only showed

some overlap in their signatures. To evaluate the accuracy of our source group differentiation, each source sample was evaluated as if it were the signature of the targeted suspended sediment with unknown source contributions. The model run where bank soils for each land use were classified as a separate sources was found to misclassify > 10% of samples in each land use category. Although, it should also be noted that due to the small sample size, one sample in each group being misclassified results in the overall source group being misclassified as per the Sed_SAT error analysis definition of source group misclassification. Still, a small sample size does not account for the poorly defined signatures seen in a few of the sample groups. Most notably, no individual sample in the upland developed soil group was identified as having a mostly developed land use signature and showed great variety in alleged contributing sources. This suggests that there is no strong signature unique to the upland developed soils. The source contributions assigned to samples of other source groups showed similarities between bank and upland sources of the same land use. Although the similarities in signatures between some source groups when distinguishing between upland and bank soil was a limiting factor, it was not completely unexpected and still proved to be informative. For example, the unique fingerprint of the developed bank samples was unmistakable. We were able to confidently identify the relative percentage each land use contributed to the suspended sediment and further conclude that the urban source signal was primarily from stream banks in developed areas.

2.03.7 Implications and Future Directions

While the land use category and proportion of each source group attributed to each suspended sediment sample were relatively consistent between the two runs, there were sources of uncertainty when differentiating between upland and bank soils of the same land use. The

overlap between such groups is a reflection of the similarities in their soil and geology. This is mostly due to the scale of this study. However, these similarities also make differences in fingerprints more likely to be exclusively due to land use.

An expansion of this study could include other streams that feed into Lake Thunderbird to better encompass sediment sources from the whole watershed. This would also include other land uses such as pasture or rangeland and an increase in the sample size to result in a more representative sediment fingerprint for each land use. Additionally, an expansion of this project with an increased number of sediment traps could allow for adequate sample volumes to be collected on a shorter timescale such as following precipitation events. This change in sampling frequency could allow us to better characterize the origin of runoff within this sub-watershed. We observed a shift in land use contribution between October and November samples that could be investigated with a longer sampling period and attributed to either seasonal changes or precipitation events. A future study could also include stream bed samples as a source in the unmixing model. While the concentrations of tracers were measured in bed samples for comparison to suspended sediment, these were not included in the unmixing model. Finally, there are a wide variety of tracers that can be included in a sediment fingerprint. Organic matter content and fallout radionuclides have been used to differentiate between bank and upland soils in other source tracing studies and could be applied here (Fox & Papanicolaou, 2008;).

2.04 Conclusions

In conclusion, an unmixing model was used to assess the source of the sediment loading in Dave Blue Creek which contributes to problems with water quality in Lake Thunderbird. Dave

Blue Creek was shown to have contributions from all three land uses with grasslands contributing the majority in the sediment samples collected over the first two months and developed samples consistently appearing in all three suspended sediment samples. Notably, the change in land use contributions to suspended sediment over the sampling period corresponded with changes in discharge and precipitation within the study area. While the accuracy land use contributions were well supported, similar signatures between bank and upland samples resulted in uncertainty whether the grassland and forest contributions were from surface runoff or channel erosion. However, the developed bank samples were better defined than upland bank sources and were most likely responsible for the reoccurring developed sediment contribution in Dave Blue Creek. Future erosion mitigation strategies in Norman, Oklahoma should focus on bank stability in developed areas such as retaining walls where there is active construction.

BIBLIOGRAPHY

Andrino, A., Guggenberger, G., Kernchen, S., Mikutta, R., Sauheitl, L., & Boy, J. (2021). Production of Organic Acids by Arbuscular Mycorrhizal Fungi and Their Contribution in the Mobilization of Phosphorus Bound to Iron Oxides. Frontiers in Plant Science, 12, 661842. https://doi.org/10.3389/fpls.2021.661842

Allegretta, I., Legrand, S., Alfeld, M., Gattullo, C. E., Porfido, C., Spagnuolo, M., Janssens, K., & Terzano, R. (2022). SEM-EDX hyperspectral data analysis for the study of soil aggregates. *Geoderma*, *406*, 115540. https://doi.org/10.1016/j.geoderma.2021.115540

Blake, W. H., Boeckx, P., Stock, B. C., Smith, H. G., Bodé, S., Upadhayay, H. R., Gaspar, L., Goddard, R., Lennard, A. T., Lizaga, I., Lobb, D. A., Owens, P. N., Petticrew, E. L., Kuzyk, Z. Z. A., Gari, B. D., Munishi, L., Mtei, K., Nebiyu, A., Mabit, L., … Semmens, B. X. (2018). A deconvolutional Bayesian mixing model approach for river basin sediment source apportionment. Scientific Reports, 8(1), 13073. https://doi.org/10.1038/s41598-018-30905-9

Boudot, J. P., Hadj^Brahim, A. B., Steiman, R., & Seigle-Murandi, F. (1989). Biodegradation of synthetic organo-metallic complexes of iron and aluminium with selected metal to carbon ratios. *Soil Biology and Biochemistry*, *21*(7), 961–966. https://doi.org/10.1016/0038-0717(89)90088-6

Bramble, D. S. E., Ulrich, S., Schöning, I., Mikutta, R., Brandt, L., Poll, C., Kandeler, E., Mikutta, C., Konrad, A., Siemens, J., Yang, Y., Polle, A., Schall, P., Ammer, C., Kaiser, K., & Schrumpf, M. (2024). Formation of mineral-associated organic matter in temperate soils is primarily controlled by mineral type and modified by land use and management intensity. Global Change Biology, 30(1), e17024. https://doi.org/10.1111/gcb.17024

Brangarí, A. C., Lyonnard, B., & Rousk, J. (2022). Soil depth and tillage can characterize the soil microbial responses to drying-rewetting. *Soil Biology and Biochemistry*, *173*, 108806. https://doi.org/10.1016/j.soilbio.2022.108806

Castellano, M.J., Mueller, K.E., Olk, D.C., Sawyer, J.E. and Six, J. (2015), Integrating plant litter quality, soil organic matter stabilization, and the carbon saturation concept. Glob Change Biol, 21: 3200-3209. https://doi.org/10.1111/gcb.12982

Castillioni, K., Patten, M. A., & Souza, L. (2022). Precipitation effects on grassland plant performance are lessened by hay harvest. *Scientific Reports*, *12*(1), 3282. https://doi.org/10.1038/s41598-022-06961-7

Castillioni, K., Wilcox, K., Jiang, L., Luo, Y., Jung, C. G., & Souza, L. (2020). Drought mildly reduces plant dominance in a temperate prairie ecosystem across years. *Ecology and Evolution*, *10*(13), 6702–6713. https://doi.org/10.1002/ece3.6400

Christensen, B. T. (2001). Physical fractionation of soil and structural and functional complexity in organic matter turnover: Turnover of soil organic matter. European Journal of Soil Science, 52(3), 345–353. https://doi.org/10.1046/j.1365-2389.2001.00417.x

City of Norman, OK. (2024). City of Norman Phase II MS4 Annual Report Reporting Period 7/1/2023 to 6/30/2024 Phase II Small Municipal Separate Storm Sewer System (MS4) General Permit (OKR04) Authorization No. OKR040015. https://www.normanok.gov/sites/default/files/documents/2024-10/MS4%20Annual%20Report%20FY2024%20final%20red.pdf

City of Norman, OK. (2023). Lake Thunderbird Watershed. City of Norman, OK. https://www.normanok.gov/your-government/departments/public-works/stormwater-division/lake-thunderbird-watershed

City of Norman, OK. (2016). Executive Summary- City of Norman, OK Lake Thunderbird Compliance Plan and Monitoring Plan. https://www.normanok.gov/sites/default/files/documents/2020-06/TMDL_JULY%202016%20-%20FINAL%207-12-2016%20Compressed.pdf

Chow, A. T., Ulus, Y., Huang, G., Kline, M. A., & Cheah, W. (2022). Challenges in quantifying and characterizing dissolved organic carbon: Sampling, isolation, storage, and analysis. *Journal of Environmental Quality*, *51*(5), 837–871. https://doi.org/10.1002/jeq2.20392

Collins, A. L., Blackwell, M., Boeckx, P., Chivers, C.-A., Emelko, M., Evrard, O., Foster, I., Gellis, A., Gholami, H., Granger, S., Harris, P., Horowitz, A. J., Laceby, J. P., Martinez-Carreras, N., Minella, J., Mol, L., Nosrati, K., Pulley, S., Silins, U., … Zhang, Y. (2020). Sediment source fingerprinting: Benchmarking recent outputs, remaining challenges and emerging themes. Journal of Soils and Sediments, 20(12), 4160–4193. https://doi.org/10.1007/s11368-020-02755-4

Collins, A. L., Pulley, S., Foster, I. D. L., Gellis, A., Porto, P., & Horowitz, A. J. (2017). Sediment source fingerprinting as an aid to catchment management: A review of the current state of knowledge and a methodological decision-tree for end-users. Journal of Environmental Management, 194, 86–108. https://doi.org/10.1016/j.jenvman.2016.09.075

Collins, A. L., Zhang, Y., McChesney, D., Walling, D. E., Haley, S. M., & Smith, P. (2012). Sediment source tracing in a lowland agricultural catchment in southern England using a modified procedure combining statistical analysis and numerical modelling. Science of The Total Environment, 414, 301–317. https://doi.org/10.1016/j.scitotenv.2011.10.062

Cotrufo, M. F., & Lavallee, J. M. (2021). Soil organic matter formation, persistence, and functioning: A synthesis of current understanding to inform its conservation and regeneration. *Advances in Agronomy*, 1–66. https://doi.org/10.1016/bs.agron.2021.11.002

Cotrufo, M. F., Ranalli, M. G., Haddix, M. L., Six, J., & Lugato, E. (2019). Soil carbon storage informed by particulate and mineral-associated organic matter. *Nature Geoscience*, *12*(12), 989–994. https://doi.org/10.1038/s41561-019-0484-6

Coward, E. K., Thompson, A., & Plante, A. F. (2018). Contrasting Fe speciation in two humid forest soils: Insight into organomineral associations in redox-active environments. *Geochimica et Cosmochimica Acta*, *238*, 68–84. https://doi.org/10.1016/j.gca.2018.07.007

Coward, E. K., Thompson, A. T., & Plante, A. F. (2017). Iron-mediated mineralogical control of organic matter accumulation in tropical soils. *Geoderma*, *306*, 206–216. https://doi.org/10.1016/j.geoderma.2017.07.026

Daily Data Retrieval. (2025, March 10). Mesonet. https://www.mesonet.org/past-data/mesonet-resources/daily-data-retrieval?ref=1778

Deng, L., Peng, C., Kim, D.-G., Li, J., Liu, Y., Hai, X., Liu, Q., Huang, C., Shangguan, Z., & Kuzyakov, Y. (2021). Drought effects on soil carbon and nitrogen dynamics in global natural ecosystems. Earth-Science Reviews, 214, 103501. https://doi.org/10.1016/j.earscirev.2020.103501

National Land Cover Database (NLCD). (2023) Multi-Resolution Land Characteristics (MRLC) consortium. https://www.mrlc.gov/viewer/

Diel, J., Vogel, H.-J., & Schlüter, S. (2019). Impact of wetting and drying cycles on soil structure dynamics. *Geoderma*, *345*, 63–71. https://doi.org/10.1016/j.geoderma.2019.03.018

Dohnalkova, A., Kovarik, L., Varga, T., Battu, A. K., Marcus, M. A., Krivanek, O., Lovejoy, T., & Kukkadapu, R. (2020). Revealing Soil Organic Matter-mineral Associations with Advanced Chemical Imaging Methods. *Microscopy and Microanalysis*, *26*(S2), 814–815. https://doi.org/10.1017/s1431927620015937

Environmental Protection Agency. (2024, April 21). EPA. https://swcweb.epa.gov/stormwatercalculator/

Fatahi, A., Gholami, H., Esmaeilpour, Y., & Fathabadi, A. (2022). Fingerprinting the spatial sources of fine-grained sediment deposited in the bed of the Mehran River, southern Iran. Scientific Reports, 12(1), 3880. https://doi.org/10.1038/s41598-022-07882-1

Fox, J.F., & K., M. D. (2015). Sediment Fingerprinting for Calibrating a Soil Erosion and Sediment-Yield Model in Mixed Land-Use Watersheds. Journal of Hydrologic Engineering, 20(6), C4014002. https://doi.org/10.1061/(asce)he.1943-5584.0001011

Fox, P. M., Nico, P. S., Tfaily, M. M., Heckman, K., & Davis, J. A. (2017). Characterization of natural organic matter in low-carbon sediments: Extraction and analytical approaches. *Organic Geochemistry*, *114*, 12–22. https://doi.org/10.1016/j.orggeochem.2017.08.009

Fox, J. F., & Papanicolaou, A. N. (2008). Application of the spatial distribution of nitrogen stable isotopes for sediment tracing at the watershed scale. Journal of Hydrology, 358(1–2), 46–55. https://doi.org/10.1016/j.jhydrol.2008.05.032

Gabriel, C. E., Kellman, L., & Prest, D. (2018). Examining mineral-associated soil organic matter pools through depth in harvested forest soil profiles. *PLoS ONE*, *13*(11), e0206847. https://doi.org/10.1371/journal.pone.0206847

Gellis, Al., Fitzpatrick F., Schubauer-Berigan, J. (2016). A Manual to Identify Sources of Fluvial Sediment. U.S. *Environmental Protection Agency*. Washington, DC, EPA/600/R-16/210

Gellis, Al., Fitzpatrick F., Schubauer-Berigan, J. (2017). Determining the sources of fine-grained sediment using the Sediment Source Assessment Tool (Sed_SAT). *Maryland Water Science Center.* https://doi.org/10.3133/ofr20171062

Gellis, Al., Fitzpatrick F., Schubauer-Berigan, J. (2017). Sediment Source Assessment Tool (Sed_SAT). *Maryland Water Science Center.* https://doi.org/ 10.5066/F76Q1VBX

Giannetta, B., Zaccone, C., Plaza, C., Siebecker, M. G., Rovira, P., Vischetti, C., & Sparks, D. L. (2019). The role of Fe(III) in soil organic matter stabilization in two size fractions having opposite features. *Science of The Total Environment*, *653*, 667–674. https://doi.org/10.1016/j.scitotenv.2018.10.361

Gross, C. D., & Harrison, R. B. (2019). The Case for Digging Deeper: Soil Organic Carbon Storage, Dynamics, and Controls in Our Changing World. *Soil Systems*, *3*(2), 28. https://doi.org/10.3390/soilsystems3020028

Guzmán, G., Quinton, J. N., Nearing, M. A., Mabit, L., & Gómez, J. A. (2013). Sediment tracers in water erosion studies: current approaches and challenges. Journal of Soils and Sediments, 13(4), 816–833. https://doi.org/10.1007/s11368-013-0659-5

Habibi, S., Gholami, H., Fathabadi, A., & Jansen, J. D. (2019). Fingerprinting sources of reservoir sediment via two modelling approaches. *Science of The Total Environment*, *663*, 78–96. https://doi.org/10.1016/j.scitotenv.2019.01.327

Haddix, M. L., Gregorich, E. G., Helgason, B. L., Janzen, H., Ellert, B. H., & Cotrufo, M. F. (2020). Climate, carbon content, and soil texture control the independent formation and persistence of particulate and mineral-associated organic matter in soil. *Geoderma*, *363*, 114160. https://doi.org/10.1016/j.geoderma.2019.114160

Harris, D., Horwáth, W. R., & Kessel, C. van. (2001). Acid fumigation of soils to remove carbonates prior to total organic carbon or CARBON-13 isotopic analysis. *Soil Science Society of America Journal*, *65*(6), 1853–1856. https://doi.org/10.2136/sssaj2001.1853

Heckman, K., Lawrence, C. R., & Harden, J. W. (2018). A sequential selective dissolution method to quantify storage and stability of organic carbon associated with Al and Fe hydroxide phases. *Geoderma*, *312*, 24–35. https://doi.org/10.1016/j.geoderma.2017.09.043

Helbling, E., Pierson, D., & Lajtha, K. (2021). Sources of soil carbon loss during soil density fractionation: Laboratory loss or seasonally variable soluble pools? *Geoderma*, *382*, 114776. https://doi.org/10.1016/j.geoderma.2020.114776

Just, C., Armbruster, M., Barkusky, D., Baumecker, M., Diepolder, M., Döring, T. F., Heigl, L., Honermeier, B., Jate, M., Merbach, I., Rusch, C., Schubert, D., Schulz, F., Schweitzer, K., Seidel, S., Sommer, M., Spiegel, H., Thumm, U., Urbatzka, P., … Wiesmeier, M. (2023). Soil organic carbon sequestration in agricultural long-term field experiments as derived from particulate and mineral-associated organic matter. Geoderma, 434, 116472. https://doi.org/10.1016/j.geoderma.2023.116472

Karra, Kontgis, et al. "Global land use/land cover with Sentinel-2 and deep learning." (2021). IGARSS 2021 IEEE International Geoscience and Remote Sensing Symposium. https://ic.imagery1.arcgis.com/arcgis/rest/services/Sentinel2_10m_LandCover/ImageServer

Kleber, M., Sollins, P., & Sutton, R. (2007). A conceptual model of organo-mineral interactions in soils: self-assembly of organic molecular fragments into zonal structures on mineral surfaces. *Biogeochemistry*, *85*(1), 9–24. https://doi.org/10.1007/s10533-007-9103-5

Koiter, A. J., Owens, P. N., Petticrew, E. L., & Lobb, D. A. (2013). The behavioural characteristics of sediment properties and their implications for sediment fingerprinting as an approach for identifying sediment sources in river basins. Earth-Science Reviews, 125, 24–42. https://doi.org/10.1016/j.earscirev.2013.05.009

Lehmann, J., & Kleber, M. (2015). The contentious nature of soil organic matter. *Nature*, *528*(7580), 60–68. https://doi.org/10.1038/nature16069

Li, Q., Hu, W., Li, L., & Li, Y. (2023). Interactions between organic matter and Fe oxides at soil micro-interfaces: Quantification, associations, and influencing factors. *Science of The Total Environment*, *855*, 158710. https://doi.org/10.1016/j.scitotenv.2022.158710

Lopez-Sangil, L., & Rovira, P. (2013). Sequential chemical extractions of the mineral-associated soil organic matter: An integrated approach for the fractionation of organo-mineral complexes. *Soil Biology and Biochemistry*, *62*, 57–67. https://doi.org/10.1016/j.soilbio.2013.03.004

Mack, S. C., Rabenhorst, M. C., & Berkowitz, J. F. (2019). Understanding the Inhibition of Color Change in Problematic Red Parent Material Hydric Soils. Soil Science Society of America Journal, 83(3), 838–847. https://doi.org/10.2136/sssaj2018.10.0390

Mayer, M., Leifeld, J., Szidat, S., Mäder, P., Krause, H.-M., & Steffens, M. (2023). Dynamic stability of mineral-associated organic matter: Enhanced stability and turnover through organic fertilization in a temperate agricultural topsoil. Soil Biology and Biochemistry, 184. https://doi.org/10.1016/j.soilbio.2023.109095

Menon, M., Mawodza, T., Rabbani, A., Blaud, A., Lair, G. J., Babaei, M., Kercheva, M., Rousseva, S., & Banwart, S. (2020). Pore system characteristics of soil aggregates and their relevance to aggregate stability. *Geoderma*, *366*, 114259. https://doi.org/10.1016/j.geoderma.2020.114259

Mikutta, R., Turner, S., Schippers, A., Gentsch, N., Meyer-Stüve, S., Condron, L. M., Peltzer, D. A., Richardson, S. J., Eger, A., Hempel, G., Kaiser, K., Klotzbücher, T., & Guggenberger, G. (2019). Microbial and abiotic controls on mineral-associated organic matter in soil profiles along an ecosystem gradient. *Scientific Reports*, *9*(1), 10294. https://doi.org/10.1038/s41598-019-46501-4

Miller, J. R., Mackin, G., Orbock Miller, M. (2015) *Application of Geochemical Tracers to Fluvial Sediment.* Springer Cham, https://doi.org/10.1007/978-3-319-13221-1

Mirabito, A. J., & Chambers, L. G. (2023). Quantifying mineral-associated organic matter in wetlands as an indicator of the degree of soil carbon protection. *Geoderma*, *430*, 116327. https://doi.org/10.1016/j.geoderma.2023.116327

Moore, D. M., & Reynolds, R. C. (1997). Chapter 6 Sample Preparation for Clay Minerals. In X-ray diffraction and the identification and analysis of Clay Minerals (pp. 205–210). essay, Oxford University Press.

Mosley, L. M., Fitzpatrick, R. W., Palmer, D., Leyden, E., & Shand, P. (2014). Changes in acidity and metal geochemistry in soils, groundwater, drain and river water in the Lower Murray River after a severe drought. Science of The Total Environment, 485, 281–291. https://doi.org/10.1016/j.scitotenv.2014.03.063

Mundende, D. C. (2010). Soil and Water Conservation, *The Encyclopedia of Oklahoma History and Culture*, https://www.okhistory.org/publications/enc/entry?entry=SO005.

Mukundan, R., Radcliffe, D. E., Ritchie, J. C., Risse, L. M., & McKinley, R. A. (2010). Sediment Fingerprinting to Determine the Source of Suspended Sediment in a Southern Piedmont Stream. Journal of Environmental Quality, 39(4), 1328–1337. https://doi.org/10.2134/jeq2009.0405

Nosrati, K., Akbari-Mahdiabad, M., Fiener, P., & Collins, A. L. (2021). Using different size fractions to source fingerprint fine-grained channel bed sediment in a large drainage basin in Iran. CATENA, 200, 105173. https://doi.org/10.1016/j.catena.2021.105173

Oklahoma Water Resource Board. (2024). *OWRB Water Data and Analysis Tools Dashboard*. https://data-owrb.aquaticinformatics.net/Data

Patault, E., Alary, C., Franke, C., & Abriak, N.-E. (2019). Quantification of tributaries contributions using a confluence-based sediment fingerprinting approach in the Canche river watershed (France). *Science of The Total Environment*, *668*, 457–469. https://doi.org/10.1016/j.scitotenv.2019.02.458

Patzner, M. S., Mueller, C. W., Malusova, M., Baur, M., Nikeleit, V., Scholten, T., Hoeschen, C., Byrne, J. M., Borch, T., Kappler, A., & Bryce, C. (2020). Iron mineral dissolution releases iron and associated organic carbon during permafrost thaw. *Nature Communications*, *11*(1), 6329. https://doi.org/10.1038/s41467-020-20102-6

Perks, M. T., Warburton, J., & Bracken, L. (2014). Critical assessment and validation of a time-integrating fluvial suspended sediment sampler. *Hydrological Processes*, *28*(17), 4795–4807. https://doi.org/10.1002/hyp.9985

Phillips, J. M., Russell, M. A., & Walling, D. E. (2000). Time-integrated sampling of fluvial suspended sediment: A simple methodology for small catchments. Hydrological Processes, 14(14), 2589–2602. https://doi.org/10.1002/1099-1085(20001015)14:14<2589::aid-hyp94>3.0.co;2-d

Poeplau, C., Don, A., Six, J., Kaiser, M., Benbi, D., Chenu, C., Cotrufo, M. F., Derrien, D., Gioacchini, P., Grand, S., Gregorich, E., Griepentrog, M., Gunina, A., Haddix, M., Kuzyakov, Y., Kühnel, A., Macdonald, L. M., Soong, J., Trigalet, S., … Nieder, R. (2018). Isolating organic carbon fractions with varying turnover rates in temperate agricultural soils – A comprehensive method comparison. *Soil Biology and Biochemistry*, *125*, 10–26. https://doi.org/10.1016/j.soilbio.2018.06.025

Pulley, S., Foster, I., & Collins, A. L. (2017). The impact of catchment source group classification on the accuracy of sediment fingerprinting outputs. Journal of Environmental Management, 194, 16–26. https://doi.org/10.1016/j.jenvman.2016.04.048

Rakhsh, F., Golchin, A., Beheshti Al Agha, A., & Alamdari, P. (2017). Effects of exchangeable cations, mineralogy and clay content on the mineralization of plant residue carbon. Geoderma, 307, 150–158. https://doi.org/10.1016/j.geoderma.2017.07.010

Rasmussen, C., Heckman, K., Wieder, W. R., Keiluweit, M., Lawrence, C. R., Berhe, A. A., Blankinship, J. C., Crow, S. E., Druhan, J. L., Pries, C. E. H., Marin-Spiotta, E., Plante, A. F., Schädel, C., Schimel, J. P., Sierra, C. A., Thompson, A., & Wagai, R. (2018). Beyond clay: towards an improved set of variables for predicting soil organic matter content. *Biogeochemistry*, *137*(3), 297–306. https://doi.org/10.1007/s10533-018-0424-3

Rasmussen, C., Southard, R. J., & Horwath, W. R. (2006). Mineral control of organic carbon mineralization in a range of temperate conifer forest soils. *Global Change Biology*, *12*(5), 834–847. https://doi.org/10.1111/j.1365-2486.2006.01132.x

Ritson, J. P., Graham, N. J. D., Templeton, M. R., Clark, J. M., Gough, R., & Freeman, C. (2014). The impact of climate change on the treatability of dissolved organic matter (DOM) in upland water supplies: A UK perspective. Science of The Total Environment, 473–474, 714–730. https://doi.org/10.1016/j.scitotenv.2013.12.095

Rocci, K. S., Lavallee, J. M., Stewart, C. E., & Cotrufo, M. F. (2021). Soil organic carbon response to global environmental change depends on its distribution between mineral-

associated and particulate organic matter: A meta-analysis. *Science of The Total Environment*, *793*, 148569. https://doi.org/10.1016/j.scitotenv.2021.148569

Saidy, A. R., Smernik, R. J., Baldock, J. A., Kaiser, K., & Sanderman, J. (2013). The sorption of organic carbon onto differing clay minerals in the presence and absence of hydrous iron oxide. Geoderma, 209–210, 15–21. https://doi.org/10.1016/j.geoderma.2013.05.026

Shajib, M. T. I., Hansen, H. C. B., Liang, T., & Holm, P. E. (2020). Rare earth elements in surface specific urban runoff in Northern Beijing. *Science of The Total Environment*, *717*, 136969. https://doi.org/10.1016/j.scitotenv.2020.136969

Singh, M., Sarkar, B., Sarkar, S., Churchman, J., Bolan, N., Mandal, S., Menon, M., Purakayastha, T. J., & Beerling, D. J. (2017). Stabilization of Soil Organic Carbon as Influenced by Clay Mineralogy. *Advances in Agronomy*, 33–84. https://doi.org/10.1016/bs.agron.2017.11.001

Six, J., Elliott, E. T., & Paustian, K. (2000). Soil Structure and Soil Organic Matter II. A Normalized Stability Index and the Effect of Mineralogy. Soil Science Society of America Journal, 64(3), 1042–1049. https://doi.org/10.2136/sssaj2000.6431042x

Slotznick, S. P., Sperling, E. A., Tosca, N. J., Miller, A. J., Clayton, K. E., Helmond, N. A. G. M. van, Slomp, C. P., & Swanson-Hysell, N. L. (2020). Unraveling the Mineralogical Complexity of Sediment Iron Speciation Using Sequential Extractions. *Geochemistry, Geophysics, Geosystems*, *21*(2). https://doi.org/10.1029/2019gc008666

Souza, L. F. T., Hirmas, D. R., Sullivan, P. L., Reuman, D. C., Kirk, M. F., Li, L., Ajami, H., Wen, H., Sarto, M. V. M., Loecke, T. D., Rudick, A. K., Rice, C. W., & Billings, S. A. (2023). Root distributions, precipitation, and soil structure converge to govern soil organic carbon depth distributions. Geoderma, 437, 116569. https://doi.org/10.1016/j.geoderma.2023.116569

Sun, S., Liu, X., Lu, S., Cao, P., Hui, D., Chen, J., Guo, J., & Yang, Y. (2023). Depth-dependent response of particulate and mineral-associated organic carbon to long-term throughfall reduction in a subtropical natural forest. *CATENA*, *223*, 106904. https://doi.org/10.1016/j.catena.2022.106904

Wagai, R., & Mayer, L. M. (2007). Sorptive stabilization of organic matter in soils by hydrous iron oxides. *Geochimica et Cosmochimica Acta*, *71*(1), 25–35. https://doi.org/10.1016/j.gca.2006.08.047

Walkinshaw, Mike, A.T. O'Geen, D.E. Beaudette. "Soil Properties." *California Soil Resource Lab*, 1 Oct. 2023, casoilresource.lawr.ucdavis.edu/soil-properties/.

Walling, D. E. (2013). The evolution of sediment source fingerprinting investigations in fluvial systems. Journal of Soils and Sediments, 13(10), 1658–1675. https://doi.org/10.1007/s11368-013-0767-2

Walling, D. E., & Collins, A. L. (2008). The catchment sediment budget as a management tool. Monitoring and Modelling Diffuse Pollution from Agriculture for Policy Support: UK and European Experience., 11(2), 136–143. https://doi.org/10.1016/j.envsci.2007.10.004

Wan, S., Hui, D., Wallace, L., & Luo, Y. (2005). Direct and indirect effects of experimental warming on ecosystem carbon processes in a tallgrass prairie. *Global Biogeochemical Cycles*, *19*(2). https://doi.org/10.1029/2004GB002315

Wiesmeier, M., Poeplau, C., Sierra, C. A., Maier, H., Frühauf, C., Hübner, R., Kühnel, A., Spörlein, P., Geuß, U., Hangen, E., Schilling, B., Lützow, M. von, & Kögel-Knabner, I. (2016). Projected loss of soil organic carbon in temperate agricultural soils in the 21st century: effects of climate change and carbon input trends. *Scientific Reports*, *6*(1), 32525. https://doi.org/10.1038/srep32525

Yu, M., & Rhoads, B. L. (2018). Floodplains as a source of fine sediment in grazed landscapes: Tracing the source of suspended sediment in the headwaters of an intensively managed agricultural landscape. Geomorphology, 308, 278–292. https://doi.org/10.1016/j.geomorph.2018.01.022

Zafar, M., & Lu, S.-G. (2015). Pore Size Distribution of Clayey Soils and Its Correlation with Soil Organic Matter. *Pedosphere*, *25*(2), 240–249. https://doi.org/10.1016/s1002-0160(15)60009-1

Zhang, X. C. (John), & Liu, B. L. (2016). Using multiple composite fingerprints to quantify fine sediment source contributions: A new direction. Geoderma, 268, 108–118. https://doi.org/10.1016/j.geoderma.2016.01.031